(NASA-CR-155579) RADAR IMAGE PROCESSING MODULE DEVELOPMENT PROGRAM, PHASE 3 Final Report (Texas Instruments, Inc.) 86 p HC A05/MF A01 CSCL 17I

N78-16216

Unclas

G3/32 04170

TEXAS INSTRUMENTS
INCORPORATED

FINAL REPORT

FOR THE

RADAR IMAGE PROCESSING MODULE

DEVELOPMENT PROGRAM - PHASE III

Prepared for:

Jet Propulsion Laboratory

Equipment Group

Contract No. 954340

August 1977

TEXAS INSTRUMENTS

INCORPORATED

LIST OF ILLUSTRATIONS

TABLE OF CONTENTS

LIST OF ILLUSTRATIONS (CON'T)

LIST OF TABLES

TEXAS INSTRUMENTS INCORPORATED
EQUIPMENT GROUP
13500 North Central Expressway
P.O. Box 6015
Dallas, Texas 75222

August 1977

RADAR IMAGE PROCESSING MODULE DEVELOPMENT PROGRAM - PHASE III FINAL REPORT

Reference: Jet Propulsion Laboratory Contract No. 954340

SECTION I
INTRODUCTION AND SUMMARY

This report is the final report for Phase III of the Image Processing Module (IPM) Development Program. The major objective of the program was to demonstrate the feasibility of using charge coupled devices (CCD's) in an IPM for processing synthetic aperture radar signals onboard the NASA Convair 990 (CV990) aircraft. Specifically, the goals of the program were as follows:

- Process and display realtime synthetic aperture radar returns onboard the CV990
- Record sampled raw data for use in future testing
- Evaluate the IPM performance

Two opportunities occurred to record and process radar data onboard the CV990 - December, 1975, and August, 1976. On the first flight a CCD sampler and digital tape recorder were used to record data. Upon attempting to process the data it was discovered that several circuit problems existed in the CCD sampler that made the recorded data unusable. The sampler circuits were modified to improve operation in readiness for the 1976 flights.

Schedule problems prevented the completion of the IPM in time for the August, 1976, flights so a decision was made to fly the sampler/recorder again in an effort to accumulate raw data for use in testing the IPM. In the interest of quickly obtaining processed pictures, JPL attempted to use software processing of the data and discovered that there was a line-to-line jitter (synchronization) problem with the raw data. JPL used the computer to de-jitter several scenes of raw data and subsequently produced software processed images.

After completing the IPM, the de-jittered raw data was processed at Texas Instruments using both the IPM and a software simulation on a Texas Instruments 960A minicomputer. Although images were produced, the results were very disappointing. Considerable effort was spent testing the IPM/Sampler and in computer modeling of the CCD's in an attempt to analyze the performance of the equipment. However, the program scope and schedule did not allow for resolution of the problem.

JPL has continued to software process the de-jittered raw data and has found that the data contains a dc offset. By modifying their software, reasonable images have been produced but none were available at the time this report was published.

An investigation of the CCD Filter tap weights revealed that they exhibited a significant dc gain and thus would be highly susceptible to dc offsets in the input data set. At JPL's suggestion, the filter tap weights were modified on the Texas Instruments 960A simulation in order to minimize the effects of the offset. Processing was again repeated with some improvement in resolution but no good quality images were produced. Time did not permit a complete examination of the offset problem.

The following sections provide details on the equipment and the testing. Section II describes the equipment and Sections III and IV describe the tests and the test results. Appendix A documents the derivation of the digital presum filter and Appendix B is a paper presented at the conference on CCD Technology and Applications, (held at Washington D.C. - November 1976) which further describes the Phase II and Phase III efforts of this program. Appendix C contains photographs of the sampler/tape recorder, the realtime display, and circuit boards in the IPM.

SECTION II

EQUIPMENT DESCRIPTION

The equipment utilized by the Phase III program consists of 5 major groups:

- Sampler
- Data Storage System
- IPM
- Real Time Display
- Computer Test Set

There are 3 major operating modes of the equipment as shown in Figure 2-1. Mode 1 uses the computer test set to exercise the IPM at the subsystem level. This mode allows range and azimuth filter tests as well as other IPM circuitry tests. Mode 2 uses the sampler to time expand radar data. The time expanded radar data is sent both to the data storage system and to the IPM. The equipment actually flown in December 1975 and August 1976 did not include the IPM and real time display. The sampler and data storage system were flown in this configuration. The IPM and display were connected and the data was reproduced in the lab to checkout the IPM with real data. Mode 3 uses the 960A computer and computer test set to simulate the IPM data processing and drive the real time display.

A. SAMPLER

The sampler performs the functions of sampling and time-expanding the radar return video data. The sampler contains three CCD shift registers operating in parallel which load at a high rate (25 MHz) during the short duration radar return and unload at a much lower rate (543 KHz) over the remainder of the pulse repetition interval (PRI). The sampler length is 513 samples. A schematic diagram of the sampler is shown in Figure 2-2.

The radar provides the sampler with three signals: video data, PRF (sync) signal and STALO signal. The PRF signal is synchronized with the radar pulse transmission. The PRF signal is used by the sampler to trigger the sampling of the radar return signal. The STALO signal is a stable 5 MHz

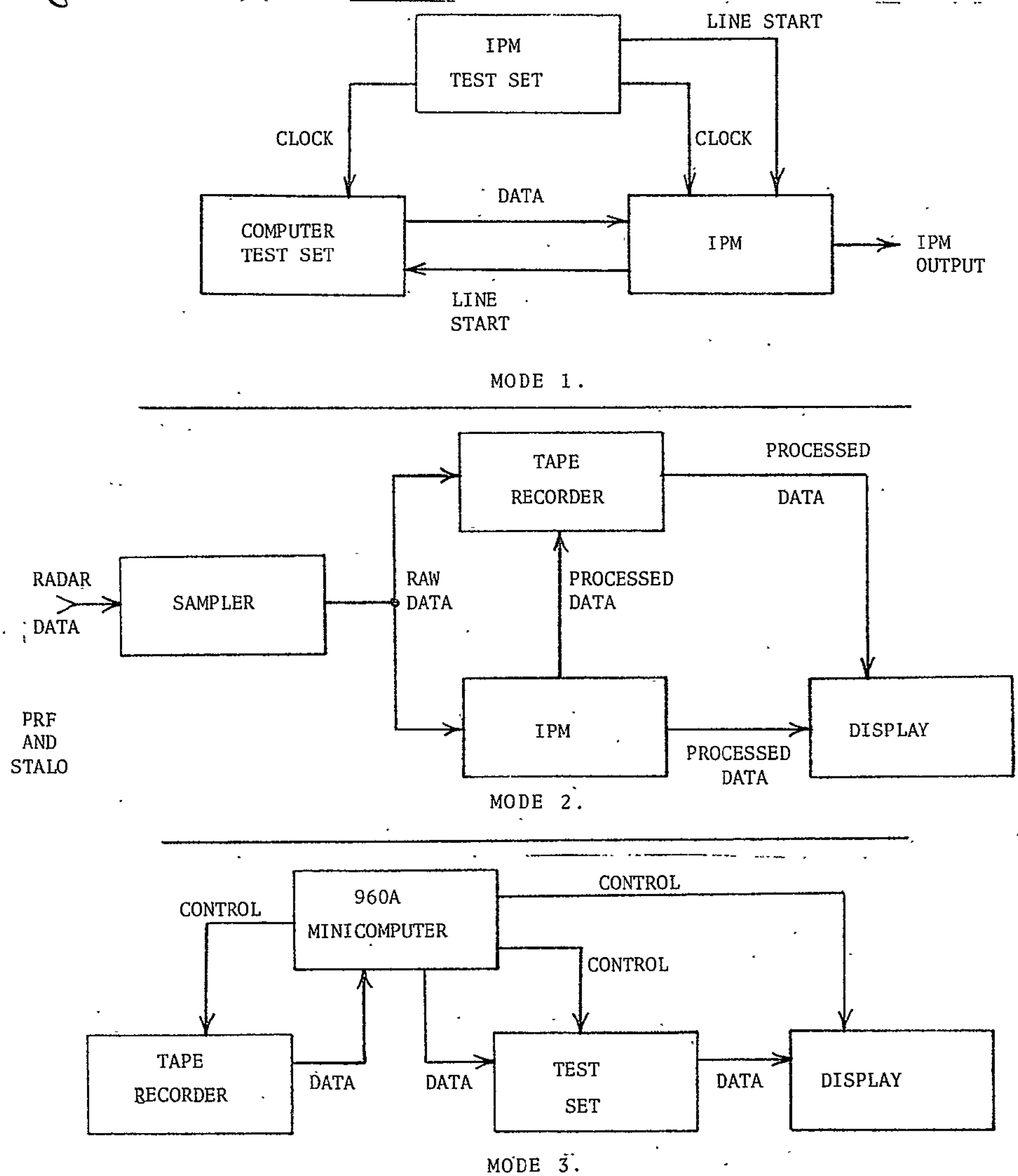

Figure 2-1. System Operational Modes

NOTES: UNLESS OTHERWISE SPECIFIED
1 REFERENCE DESIGNATION PREFIX
2 RESISTANCE VALUES ARE IN OHMS
3 CAPACITANCE VALUES ARE IN MICROFARADS
4 ON 14 PIN ICS PIN 14 IS +5V AND PIN 7 IS GND

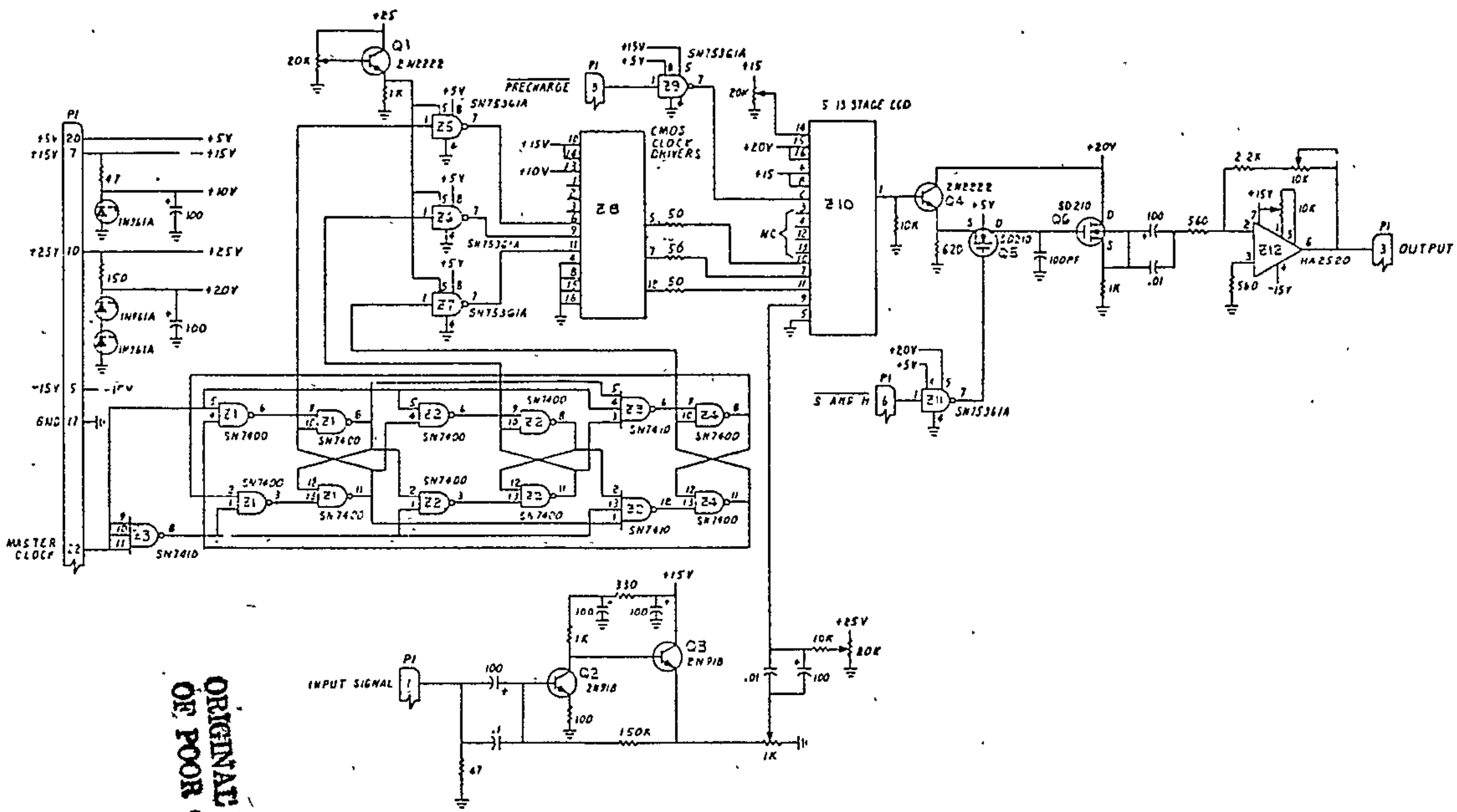

Figure 2-2. Sampler Schematic

ORIGINAL PAGE IS OF POOR QUALITY

signal used for internal timing by the radar transmitter. The STALO signal is upconverted to a 25 MHz sample frequency by a phase-locked loop in the sampler. A block diagram of the sampler timing circuitry is shown in Figure 2-3.

The particular CCD utilized in this sampler is a 3 phase multiplexed structure permitting sampling at a 25 MHz rate while the CCD clocks are operating at 8.33 MHz. This is possible because the CCD first demultiplexes the video into three parallel CCD delay lines, shifts the video down the parallel delay lines and then multiplexes the output of the three delay lines into a single output. This CCD structure is referred to as a DLM (demultiplex-linear-multiplex) device. While it has clocking advantages, it also has disadvantages in that noise is introduced into the output which is periodic with the number of multiplexed channels. This noise (for this three Channel device) is referred to as modulo-three noise which reduces dynamic range and can introduce lines on processed images.

A test set was built for lab checkout of the sampler. The test set furnishes the three input signals (PRF, STALO, and video) to the sampler. The signal is selectable between a triangular wave and a square wave and signal amplitude is variable.

B. DATA STORAGE SYSTEM

In order to lab test the IPM, it is necessary to record and reproduce the radar return video from the sampler. When available, the processed IPM output data can also be recorded concurrently with the unprocessed data. The magnetic tape recorder/reproducer chosen was a Sangamo Sabre III with PCM recording and deskewing capability. The recorder and interface electronics were bought and developed for another program. The system was borrowed for this program and modified to meet mission requirements. A block diagram of the data storage system is shown in Figure 2-4.

The Sangamo Sabre III is basically an analog magnetic tape recorder modified for digital use. The Sabre III records PCM data continuously with a fixed tape speed. In order to retrieve discrete sections of data, synchronization and identification signals must be recorded and decoded by the user. An auxiliary deskew electronics compensates for track-to-track skew of playback data. Deskewing of playback data allows parallel recording of

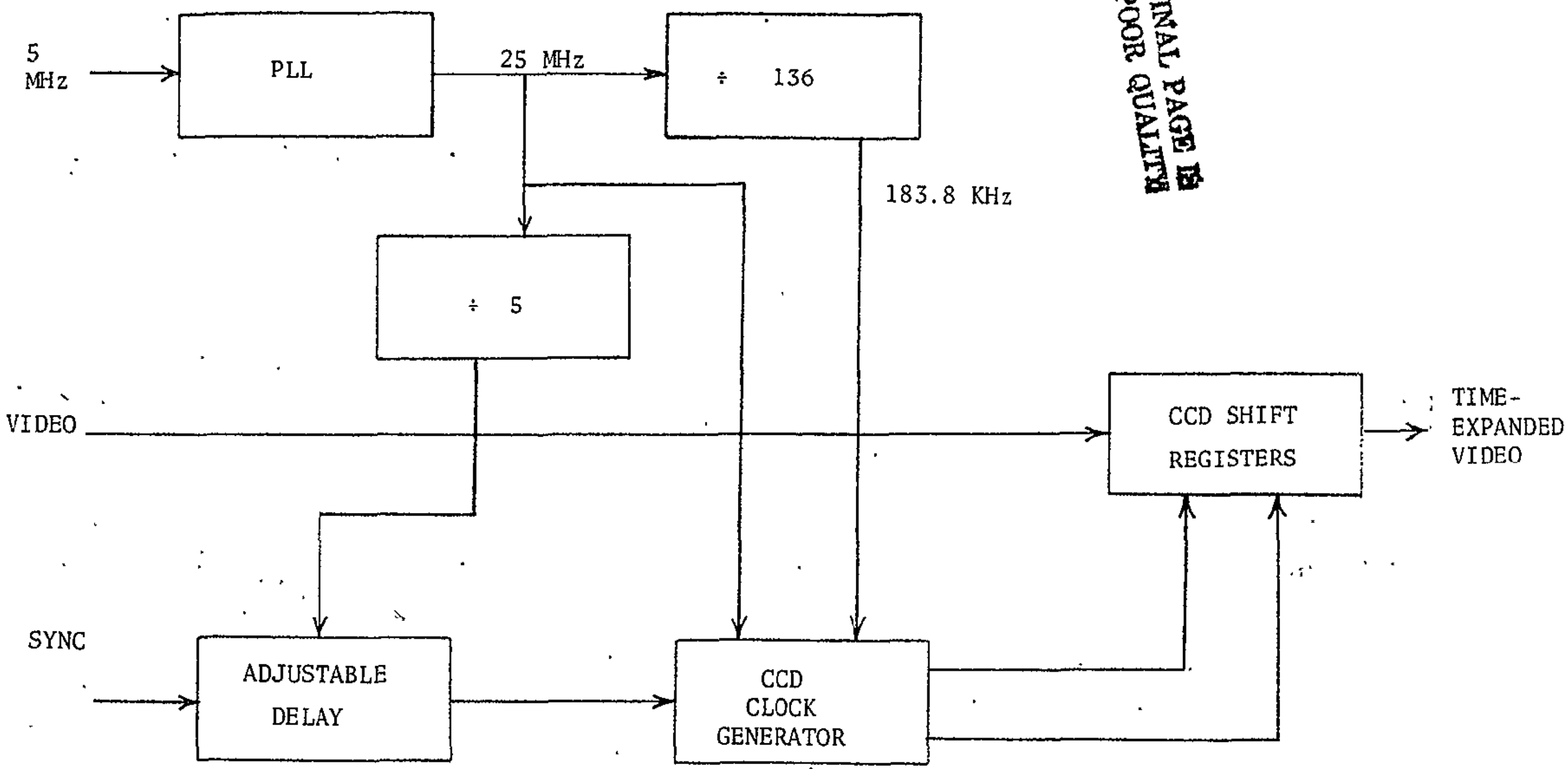

Figure 2-3. Sampler Timing Logic Block Diagram

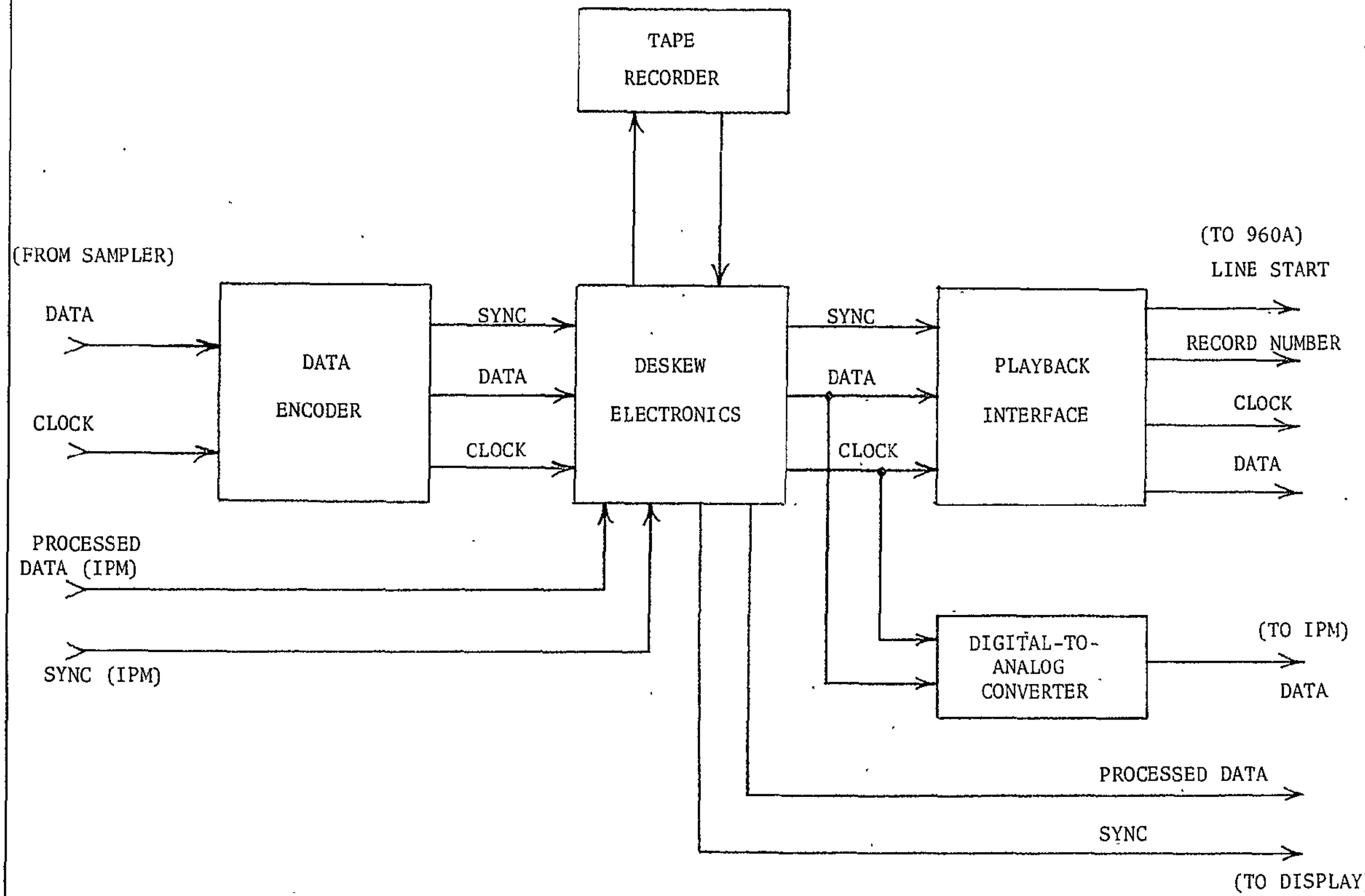

Figure 2-4. Data Storage System Block Diagram

digital data. The Sabre III used for this program has the capability to record 11 parallel PCM channels on 1 inch wide magnetic tape. Table 2-1 gives the recorder characteristics.

Table 2-1
TAPE RECORDER CHARACTERISTICS

	60 ips	1 7/8 ips
BIT PACKING DENSITIES (MIN/MAX)	12.5K/25K PER INCH	12.5K/25K
INPUT DATA RATES (MIN/MAX)	750K/1.5M	23.4K/47K
INPUT DATA RATE	1.05 MHZ	32.8 KHz
BIT ERROR RATE (MAX)	10^{-6}	10^{-5}

The basic mode of operation is to record unprocessed, time-expanded radar data on the Sangamo magnetic tape recorder on channels 1-8 at 60 ips. The video data is digitized to eight bits with a 1.05 MHz rate. Synchronization signals are recorded on channel 11. In addition, when the IPM is operational; the processed IPM output will be recorded on channel 9 with its associated sync signals on channel 10. To exercise the IPM, the stored data is reproduced at 60 ips and converted to analog. To provide software processing capability, the stored, time-expanded data on the Sabre III is reproduced at 1 7/8 ips and transferred to 9 track IBM compatible magnetic tape through some interface circuitry and a TI 960A minicomputer. The 9 track data can also be used to exercise the IPM. Previously processed IPM data may be reproduced at either 60 ips or 1 7/8 ips and fed to the real time display for viewing.

The major component of the data storage system (besides the Sangamo Sabre III) is the data encoder electronics. A block diagram of the data encoder is shown in Figure 2-5. The two signal inputs from the sampler are time expanded data and 543 KHz clock. A line start signal is generated from a voltage level detector set to trigger on the sampler load pulse. The video data is dc restored and amplified to a nominal 10 volts peak-to-peak. The data is then sampled and digitized to 8 bits at a 543 KHz rate. A 1.1 MHz (2X) clock is generated from the 543 KHz clock. The digitized data is buffered and clocked (twice per sample) to the Sangamo deskew electronics at 1.1 MHz for recording. The line start signal is used to trigger a line counter and a line start flag which are both recorded on channel 11.

IMAGE PROCESSING MODULE

The Image Processing Module (IPM) receives time-expanded radar data from the input sampler (or magnetic tape recorder) and outputs a radar elevation profile to the real-time display. For purposes of discussion and testing, the IPM is subdivided into four functional areas: range filters, presum filters, azimuth filters and magnituding circuitry. A block diagram of the IPM is shown in Figure 2-6.

The IPM is a hybrid system which uses both CCD's and digital techniques. Range correlation of the sampled radar video is performed by 32 cell CCD transversal filters. Processing of the data into pseudo real and imaginary components (I and Q respectively) is effected by processing the sampled return through a cosine filter and a sine filter which are matched to the radar chirp. After range correlation, the I and Q signals are then converted by an analog-to-digital converter into a digital format.

At this point, presum filtering in azimuth (factor of 8) of the range correlated data is performed to lower the data rate. Presum filtering also allows the subsequent azimuth correlation to be performed with a minimum azimuth correlation length and provides attenuation to the alias interference generated in the sampling process. The presum filters are implemented digitally and multiplexed between I and Q channels.

Azimuth correlation is performed by 32 cell CCD filters. One set of CCD filters is used for the I channel and one for the Q channel. The filters are used to process the entire 240 sample radar return by temporarily storing the data in a 64K MOS memory. The memory contents are read out and digital-to-

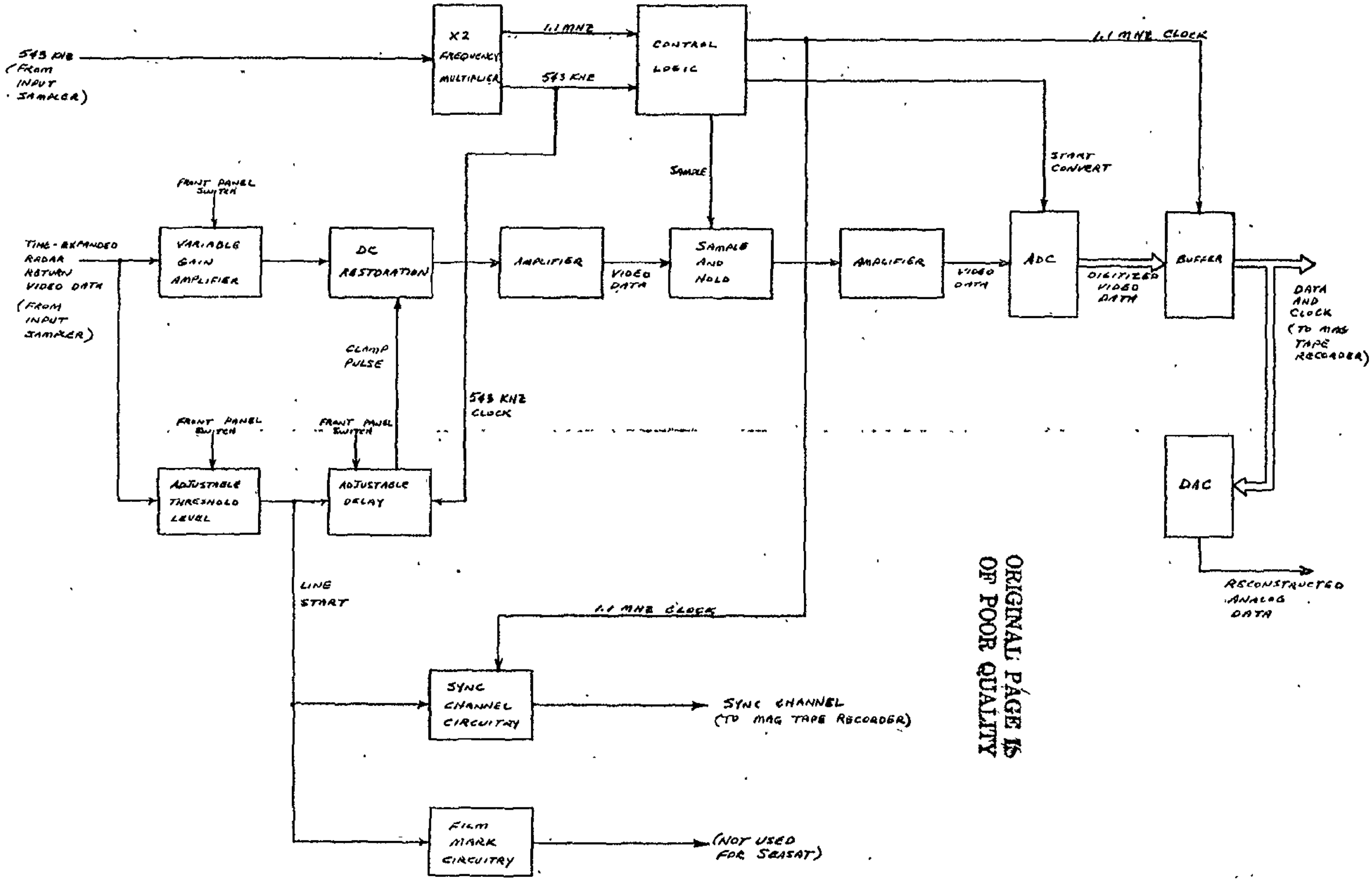

Figure 2-5. Data Encoder Block Diagram

SIZE	CODE IDENT NO	DRAWING NO
C	96214	DATA ENCODER BLOCK DIAGRAM
SCALE		SHEET

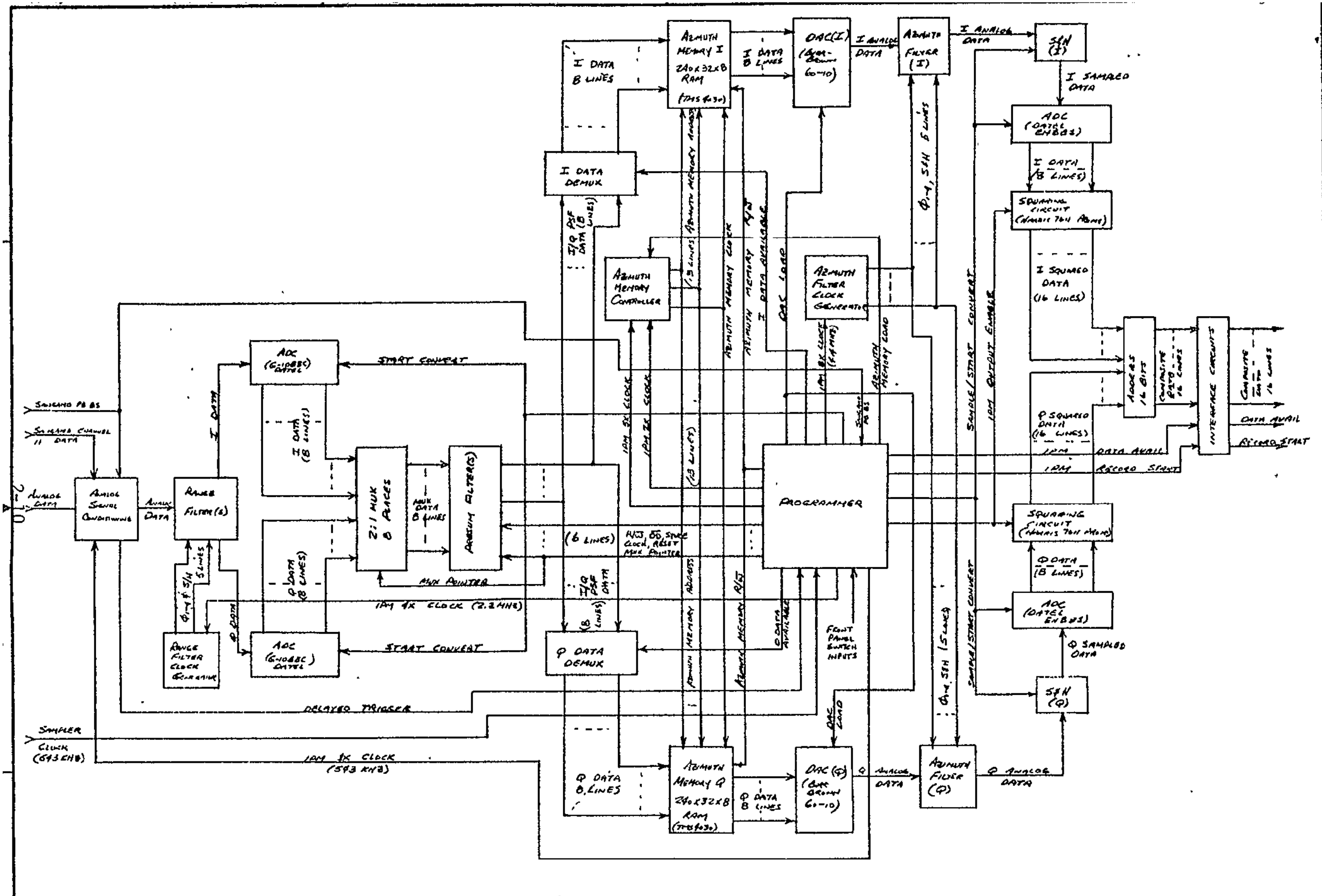

Figure 2-6. IPM Block Diagram

SIZE	CODE IDENT NO	DRAWING NO
C	96214	SEASAT PHASE III IMAGE PROCESSING MODULE BLOCK DIAGRAM
SCALE		SHEET

analog converted prior to being processed by the CCD azimuth filter. By storing the presum filter output and reading it out sequentially, the resulting azimuth processing is equivalent to the use of 240 separate parallel CCD filters for the I channel and 240 CCD filters for the Q channel. The I and Q channels are then converted into digital form by an analog-to-digital converter. The I and Q channels are squared and then summed to produce the processed output.

1. Range Filters - Range correlation of the time expanded radar return is performed by 32 cell CCD transversal filters. Processing of the data into psuedo real and imaginary components (I and Q respectively) is effected by processing the sampled return through a cosine filter and a sine filter which are matched to the radar chirp. A block diagram of the filters is shown in Figure 2-7. Outputs from the filter stages are summed by a differential current integrator. The resulting signal is sampled and held for improved signal to noise ratio and to aid the subsequent digitizing process.

The CCD transversal filters used in the IPM range filters are four phase N-channel devices with (6.0 x 0.3) mil^2 electrodes. These filters are tap weight modifications of an existing 64 stage filter design. Therefore, instead of 32 stage filters, as required for the IPM, the filters are 64 stages long with the last 31 tap weights set to zero to act only as delay stages. The filters were designed using the split electrode technique, and since phase one is the split electrode as well as the first gate of the filter, the first tap weight is also set to zero to reduce input signal feed-through. The range filters use Dolph-Chebyshev weighting to achieve 30 dB theoretical sidelobes. The tap weights of the range filter are shown in Table 2-2.

One lot (12 slices) of CCD filter bars were processed with each bar containing a sine and cosine range filter as well as a sine and cosine azimuth filter. Automatic dc testing of the entire lot indicated excellent yield had been achieved. Due to the modification of a previously designed filter the output circuitry for the filters was implemented with discrete components rather than integrated into the same substrate as the filters. The function of this output circuitry, the differential current integrator (DCI), is to provide an output voltage which is proportional to

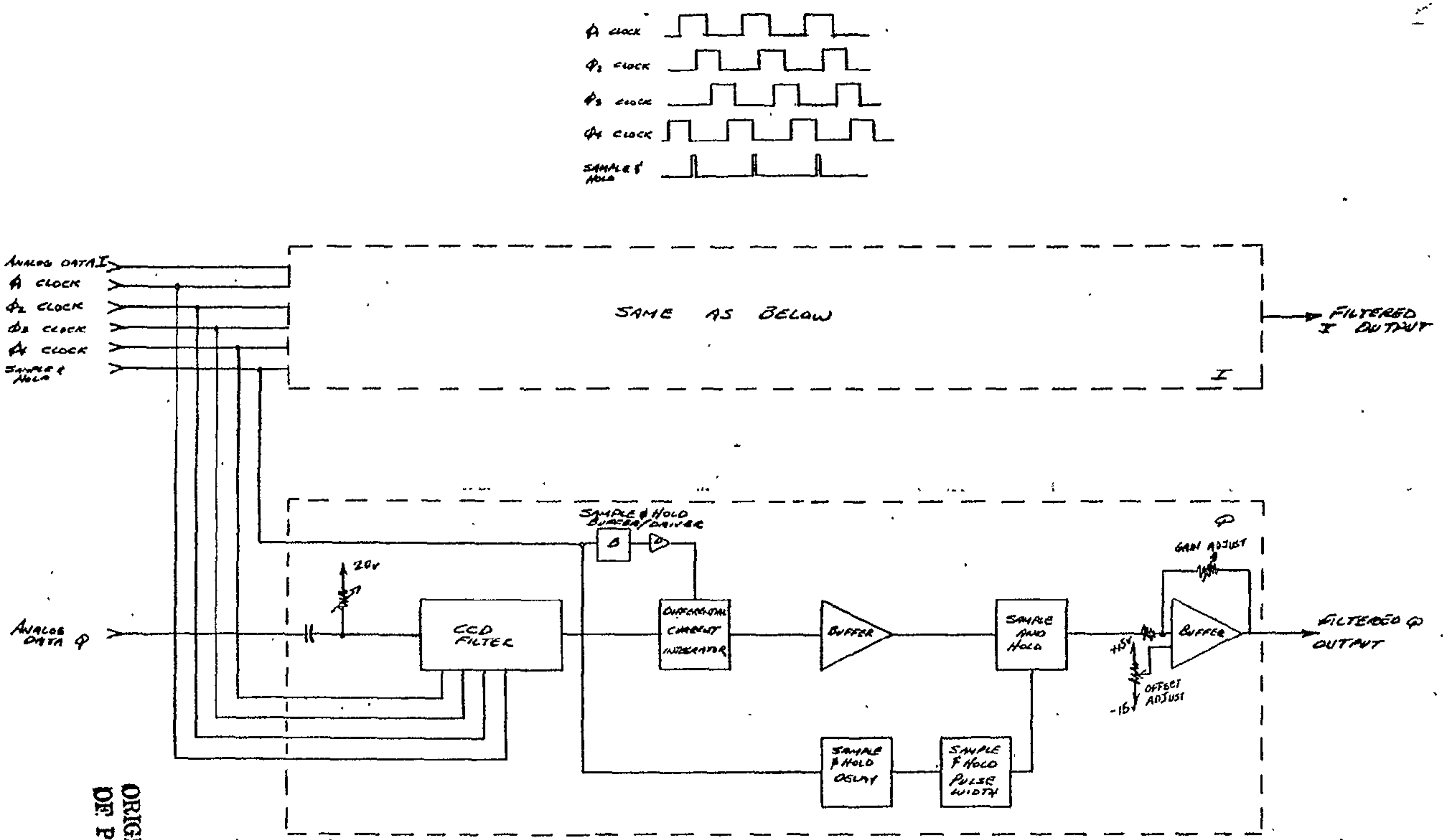

Figure 2-7. Range/Azimuth Filter Block Diagram

SIZE	CODE IDENT NO	DRAWING NO
C	96214	SEASAT III IPM RANGE/AZIMUTH FILTER BLOCK DIAGRAM
SCALE	10/20/76	SHEET

Table 2-2

RANGE FILTER TAP WEIGHTS

	COSINE	SINE
1.	433	0
2.	245	- 11
3.	303	- 53
4.	347	-141
5.	344	-283
6.	247	-456
7.	15	-592
8.	-338	-572
9.	-677	-281
10.	-753	263
11.	-348	782
12.	421	802
13.	941	95
14.	549	-807
15.	-529	-841
16.	-972	234
17.	- 3	994
18.	964	153
19.	211	-992
20.	-886	-187
21.	- 89	851
22.	795	- 69
23.	-259	-686
24.	-498	439
25.	545	231
26.	- 69	-514
27.	-325	304
28.	372	43
29.	-193	-240
30.	- 4	245
31.	254	-351

TAP WEIGHTS INCLUDE DOLPH-CHEBYSHEV WEIGHTING

VALUES ARE NORMALIZED TO 1000.

the difference in the integrated currents in the clock line segments. The design of the DCI was very critical due to the requirements for high frequencies (543 kHz) and large gains ($\geq$ 100). Precision high speed operational amplifiers were used; but, the use of many amplifiers tends to introduce noise which can limit dynamic range.

Following bonding into 28 pin dual-in-line packages, the CCD filters were functionally tested. The first test performed was the measurement of charge transfer efficiency (CTE). CTE was measured on all of the bonded devices and averaged 0.9995 per transfer. Such measurements are made from waveforms such as that in Figure 2-8 which shows the serial output response of a typical CCD filter to a rectangular pulse input.

2. Presum Filters - The function of the presum filter (digital) section is to filter the range correlated data (for both I and Q channels) in the azimuth direction. The filtered data is then stored in the I and Q azimuth memories (64K MOS RAMS), respectively. The two azimuth memories are read out sequentially, converted into analog form and presented to the I and Q azimuth filters. The digital section of the processor consists of two front-end analog-to-digital converters, a multiplexed low-pass digital filter, two sixteen kilobyte (X8) memories and two digital-to-analog converters. A block diagram of the digital section is shown in Figure 2-9.

The I and Q analog-to-digital converters quantize the range correlated data to 8 bits at a rate of 271 KHz. This rate corresponds to every second range filter output sample. Since the range filter output is a sampled waveform, the digitizing process is synchronized to the range filter sampling to eliminate the need for a second sampling. The digital data is buffered and then multiplexed for input to the presum filter.

The presum filter is a low pass, 2 pole, Butterworth filter with a 10 Hz cutoff frequency. The presum filter is implemented digitally and multiplexed between the I and Q channels. Appendix A shows the basis for the digital (powers of two) filter implementation. A functional block diagram of the presum filter is shown in Figure 2-10. Presum filtering allows a reduction in the data rate by a factor of 8. Every eighth presum filter output in each of the 240 range bins (for both I and Q) is stored in the azimuth random access memories.

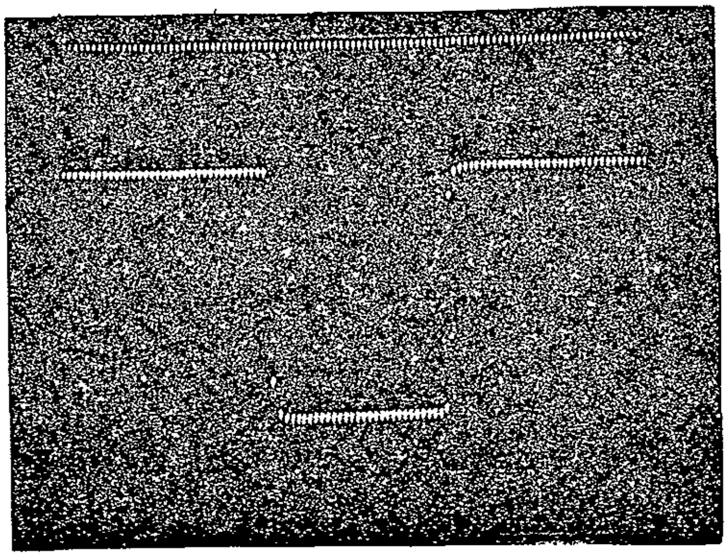

Figure 2-8. CCD Serial Output Response to
a Negative Rectangular Input Pulse

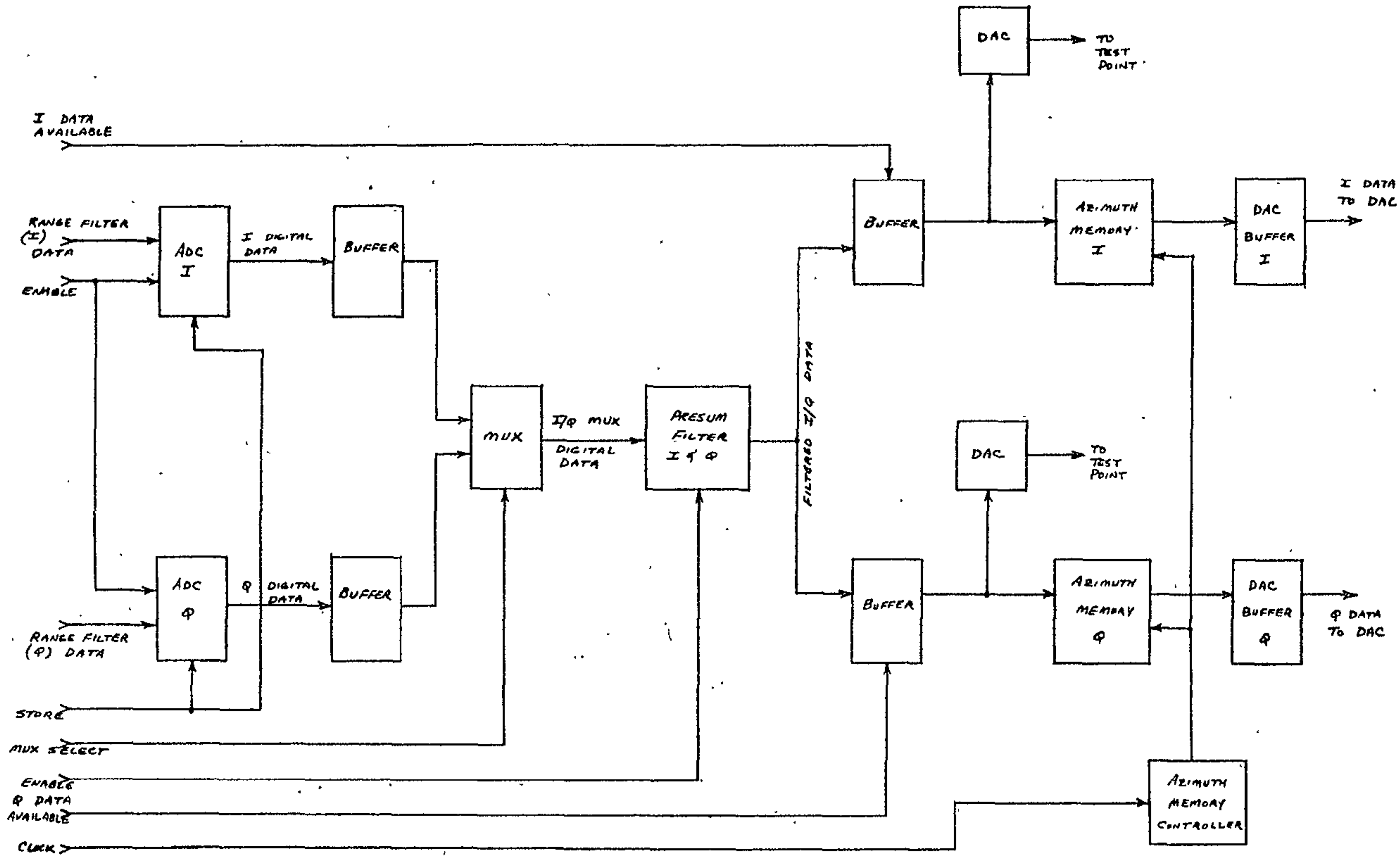

Figure 2-9. Presum Filter-Digital Section Block Diagram

SIZE	CODE IDENT NO	DRAWING NO
C	96214	DIGITAL SECTION BLOCK DIAGRAM
SCALE		SHEET

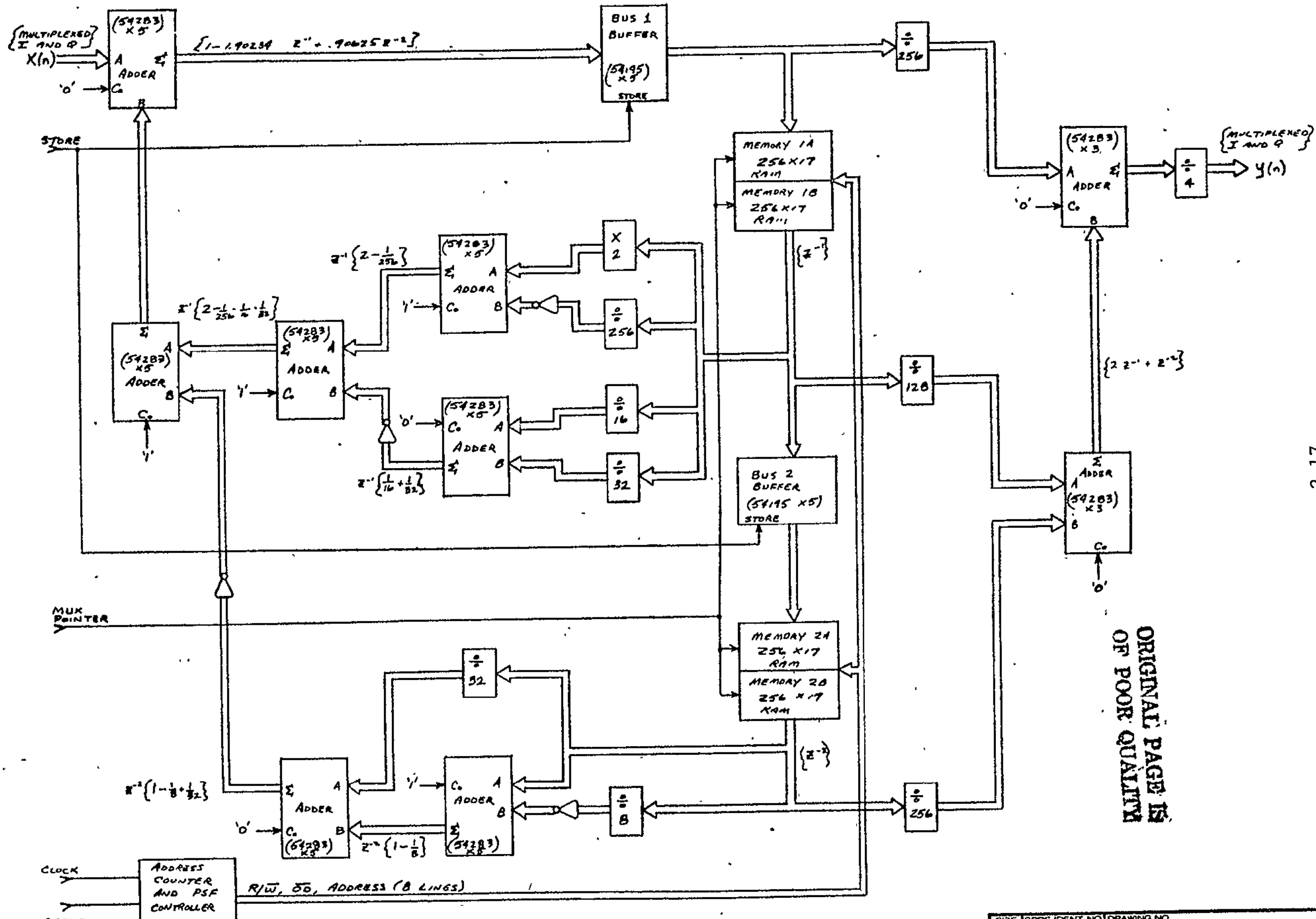

Figure 2-10. Presum Filter Block Diagram

SIZE C CODE IDENT NO 96214 DRAWING NO PRESUM FILTER BLOCK DIAGRAM SCALE SHEET

3. Azimuth Memories/Azimuth Filters - The azimuth memories are two 8K x 8 MOS random access memories. A block diagram of the azimuth memory section is shown in Figure 2-11. Each azimuth memory will contain 32 complete presum filter output range lines. The presum filter data is read into the memory cells containing the oldest data. The new data and the previous 31 data inputs are read out in chronological order for each of the 240 range bins.

The memory input data rate is 271 KHz per sample. The memory unload data rate is 1.1 MHz per sample. Unloading the entire azimuth memories requires up to 7 PRI's at the fastest radar return rate. The azimuth memory output data from each channel is converted to analog by its own digital to analog converter. The analog data is then input to the azimuth filters.

The azimuth filters operate in a similar manner to the range filters. Both filters are based on tap weight modifications of an existing filter design. The azimuth filter clock rate is 1.1 MHz. The block diagram for the range filter (Figure 2-7) is also applicable to the azimuth filter. The tap weights for the azimuth filter are shown in Table 2-3. The azimuth filters also use Dolph-Chebyshev weighting.

In operation, the filter will be loaded serially with the 32 most recent samples from each range bin and an azimuth correlation value output for that range bin will be output. The output rate will be approximately 33 KHz from the azimuth filter.

4. Magnituding Circuitry - The output of the I and Q azimuth filters must be combined to form the IPM output. The operation consists of squaring both the I and Q azimuth filter outputs and summing the squared numbers together.

The loading of the azimuth filters is done by range bin in chronological order. When all 32 samples from a range location are loaded into the filter the resulting correlation peak is sampled and digitized. The squaring and summing operations are both done digitally. The azimuth filter operation allows a reduction in data rate to one twelfth the load rate for each range location. This function is performed after the squaring and summing operations and is selectable from the IPM front panel. The squaring

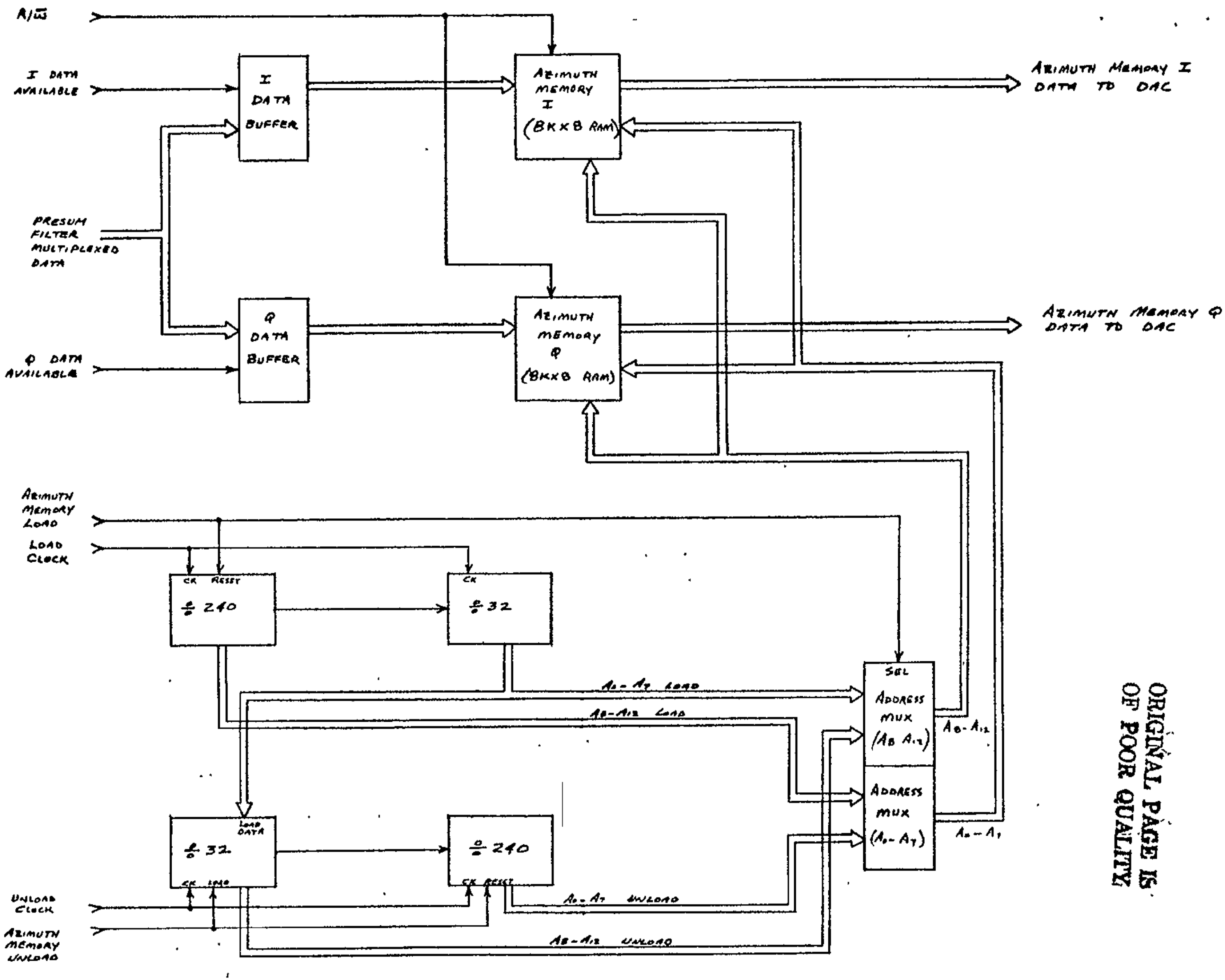

Figure 2-11. Azimuth Memory Block Diagram

Table 2-3
AZIMUTH FILTER TAP WEIGHTS

	COSINE	SINE
1.	-300	327
2.	-107	219
3.	-56	298
4.	24	368
5.	128	418
6.	247	443
7.	374	442
8.	498	416
9.	614	370
10.	717	309
11.	804	241
12.	873	172
13.	927	110
14.	964	58
15.	988	21
16.	1000	2
17.	1000	2
18.	988	21
19.	964	58
20.	927	110
21.	873	172
22.	804	241
23.	717	309
24.	614	370
25.	498	416
26.	374	442
27.	247	443
28.	128	418
29.	24	368
30.	- 56	298
31.	-107	219
32.	-300	327

TAP WEIGHTS INCLUDE DOLPH-CHEBYSHEV WEIGHTING

VALUES ARE NORMALIZED TO 1000

circuitry is implemented with a programmable read-only-memory (PROM) lookup table. The summing function is implemented with SN 54283 binary full adders. The resulting digital output (enabled for one of every 12 cycles) is sent to the real time display.

D. REAL TIME DISPLAY

The IPM output is displayed on a 9 inch TV monitor (CONRAC # ENA9/R). Interfacing the TV monitor to the IPM is done by a digital scan converter and an input interface. The scan converter output is a U.S. standard television signal.

1. Digital Scan Converter - The digital scan converter stores digital data and presents it to the TV monitor as a composite signal complete with horizontal and vertical synchronization signals, blanking etc. A block diagram of the scan converter is shown in Figure 2-12. Inputs to the scan converter are record start, data available, 8 input address lines and 4 input data lines. The scan converter memory is organized as 512 vertical lines with 240 pixels of 4 bits each. Vertical rows (range lines) are presented in chronological order from right to left (oldest data - rightmost) on the display. New data is written into the cells corresponding to the rightmost (oldest) vertical row during the horizontal flyback time. When a complete new vertical row has been written into memory, the starting vertical line address is incremented during the next vertical flyback time. This moves the newest data to the leftmost vertical line position on the display. In this way, the display will continue to update as long as data is being received. Freezing the display is done by inhibiting the data available line at the input interface. Incoming data words are supplied with a corresponding vertical address (0-239). This means the missing or extra data words will not cause the remainder of that vertical line to be offset. The scan converter memory is a 512 x 240 x 4 RAM implemented with Texas Instruments 4K x 1 dynamic RAMS (TMS 4030). The memory covers 1/2 of the full TV field area.

2. Input Interface - Data is transferred to the scan converter via the input interface. A block diagram of the input interface is shown in Figure 2-13. Three separate input data ports are provided for system operations. One port handles IPM processed data in the real time mode. A second port

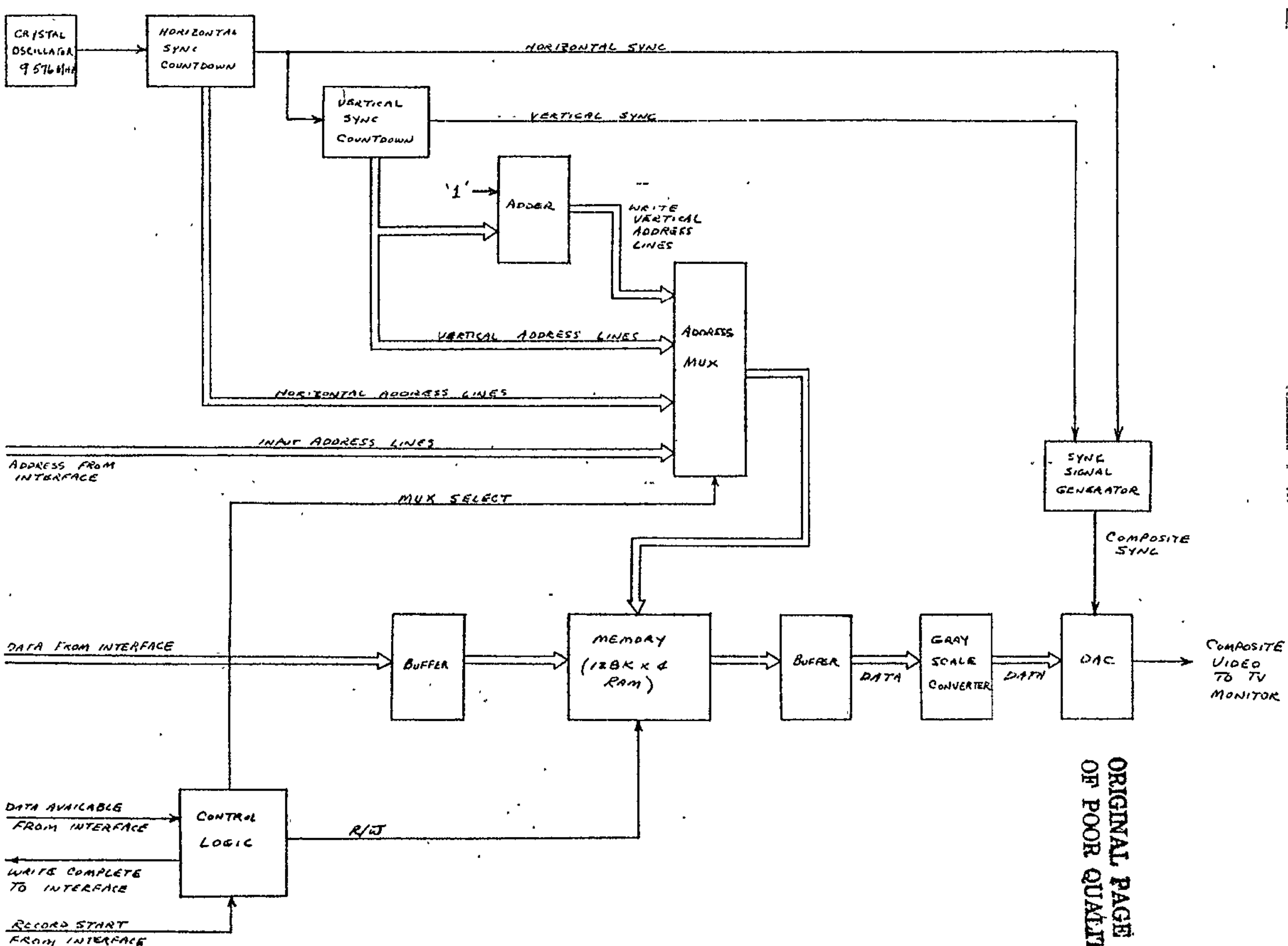

Figure 2-12. Digital Scan Converter Block Diagram

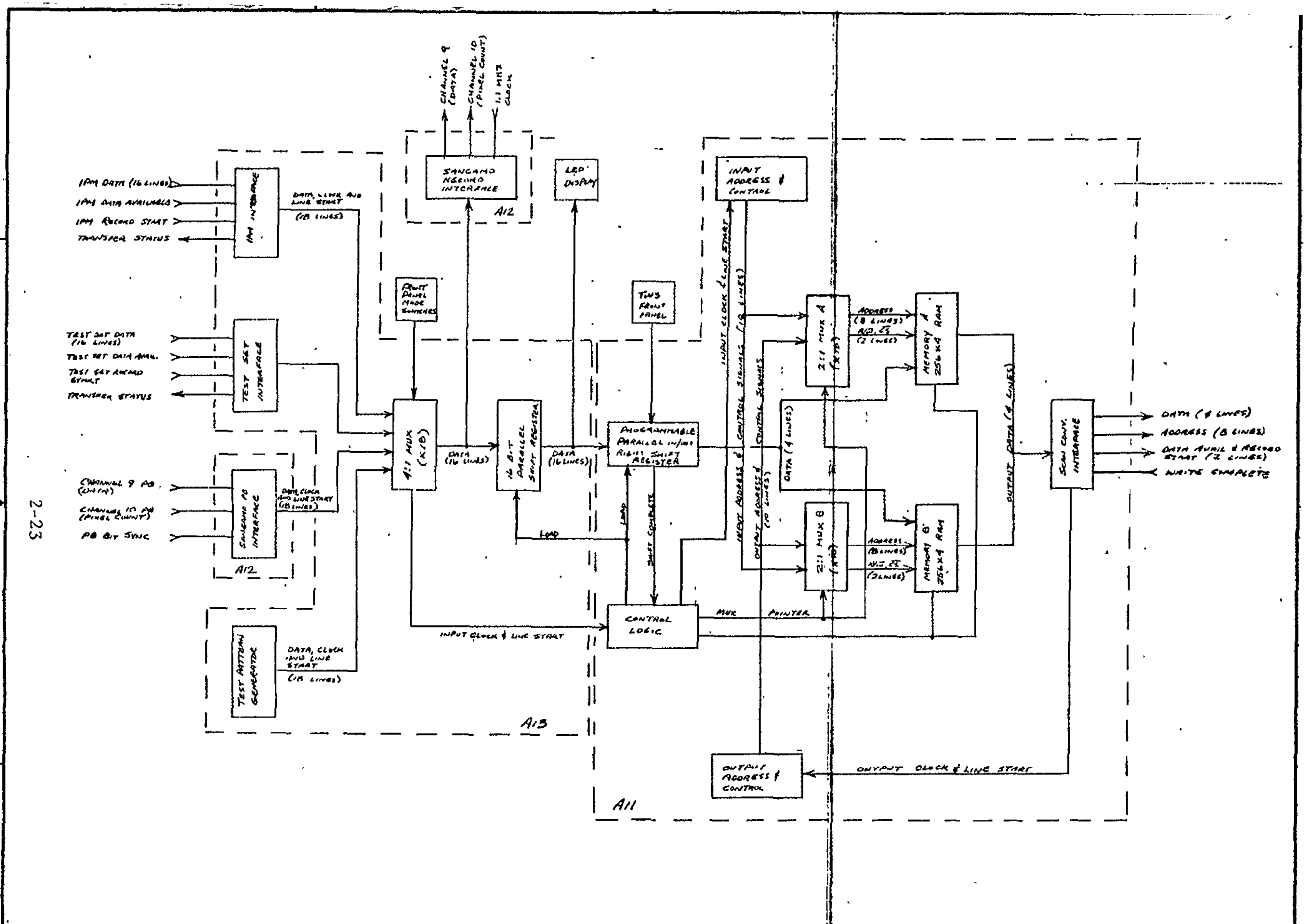

Figure 2-13. Scan Converter Interface Block Diagram

SIZE	CODE IDENT NO	DRAWING NO
C	96214	SCAN CONVERTER INTERFACE BLOCK DIAGRAM (CARDS A11, A12 & A13)
SCALE		SHEET

handles processed data in a playback mode from the Sangamo magnetic tape recorder. The remaining port displays any data transferred by the computer test set. The maximum data throughput rate is 90 K words/sec and is limited by the design constraint that new data be written into memory only during the horizontal flyback.

The input interface uses a dual buffer scheme in which a complete range line of 240 pixels is stored in one buffer while a second buffer is being emptied. The second buffer is then written into while the first is being emptied etc. Since the input data rates are considerably lower than the maximum throughput rate, the sender may control the data transfer rate.

The interfaces to the separate data sources have 16 data lines. The scan converter accepts only 4 bit data words. A cursor, selectable from the front panel points to the 4 consecutive bits to be transferred to the scan converter. LED displays monitor all 16 interface lines to facilitate proper data cursor selection. An automatic override prevents selection of too low a significant bit (and thus false presentations) by forcing the display to all white (ones) if data is present in higher ordered bit locations from those selected.

A test pattern generator is built into the input interface to provide a method of exercising the interface and scan converter without a data source. Horizontal bar patterns of gray scale, light/dark and full white or black may be selected.

SECTION III

TEST DESCRIPTIONS

A. CV990 FLIGHTS

The opportunity to record actual flight data with the L-band radar on-board the CV990 aircraft occurred in December 1975 and again in August 1976. The purpose of the December 1975 flight was to gather data in order to provide a lab test capability for the IPM prior to actually flying it in August of 1976. A CCD sampler was developed (as a modification to the Phase II contract) which enabled raw radar data to be recorded on a digital magnetic tape recorder.

1. Marineland (Dec 1975) Flights

The sampler and magnetic tape recorder were flown on the CV990 aircraft in December 1975. A series of flights, based at Patrick A.F.B. Florida were made. Several problems were encountered with the result that no usable data was recorded.

The Sangamo magnetic tape recorder had a mechanical failure in its tape transport mechanism. A pinch roller, which is part of the tape tracking mechanism suffered severe wear to its roller bearing assembly. A replacement bearing and race was installed in the field. The magnetic tape recorder was inoperative for approximately two days during the Marineland flights.

During the sampler checkout, the presence of modulo-3 noise was noted. Prior to the Marineland (December 1975) flights, it was assumed that the processing of the video data would eliminate the amplitude modulation effect of modulo-3 noise. However, data gathered using the sampler was processed by the software simulation and found to be severely degraded. The only recognizable feature was a periodic amplitude modulation pattern, three pixels wide, running in the range direction - i.e. modulo-3 noise. A subsequent analysis confirmed that the modulo-3 noise was not attenuated during processing. The modulo-3 noise problem was also aggravated by two other problems discussed in the next two paragraphs. To correct the modulo-3 noise problem a circuit was built and added to the sampler. A block diagram of the circuit is shown in Figure 3-1. Modulo-3 noise is caused by a gain mismatch between the 3 parallel sampler CCD shift registers. The correction circuit sums in one of 3 adjustable offset voltages each of which is keyed by one of the 3 CCD shift registers. A first-order correction of modulo-3 noise can be made by proper adjustment of these offset voltages. Since the magnitude of modulo-3 noise is a function of signal amplitude, the effectiveness of this fixed offset technique is limited to a small signal voltage range. For this reason, the modulo-3 correction was optimized for the lower signal levels. The sampler input amplifiers were adjusted to limit signal output voltage swing to 1 volt peak-to-peak. A compensating gain change was made both to the data encoder and to the IPM to restore the signals to their pre-modulo 3 correction amplitudes.

The modulo-3 noise problem was aggravated by two other problems. Neither problem was related to the other, but both together were sufficient to make the resulting data unusable. A communications breakdown between the IPM designers and the field crew caused the wrong 5 km swath of data to be recorded. The IPM (and the software simulation) are designed to process a 5 km swath of data beginning 5 km from nadir. This data swath is selected by an operator adjustable sampler time delay triggered by the PRF signal. The time delay required is a function of aircraft altitude. The data recorded, in all cases, included the ground return. The time delays were set incorrectly, thus recording the 5 km data swath from nadir to 5 km. This by itself is a significant problem, but if the signal amplitude is sufficient, the data can be processed.

An output from the JPL L band radar receiver which has a time-variable gain function was to have been available for use by the sampler. Instead, the only output made available to the sampler was a fixed gain output. The amplitude of the radar return (especially near nadir) is a function of both range and target size. The time-variable gain applies a first order range correction to the return. This gain equalization lowers the dynamic range requirements for the sampler and allows an effective gain increase in the swath area of interest. For the Marineland flights, the recording of the high amplitude ground return without the time variable gain meant that the sampler input amplifier gain had to be adjusted downward to accomodate the

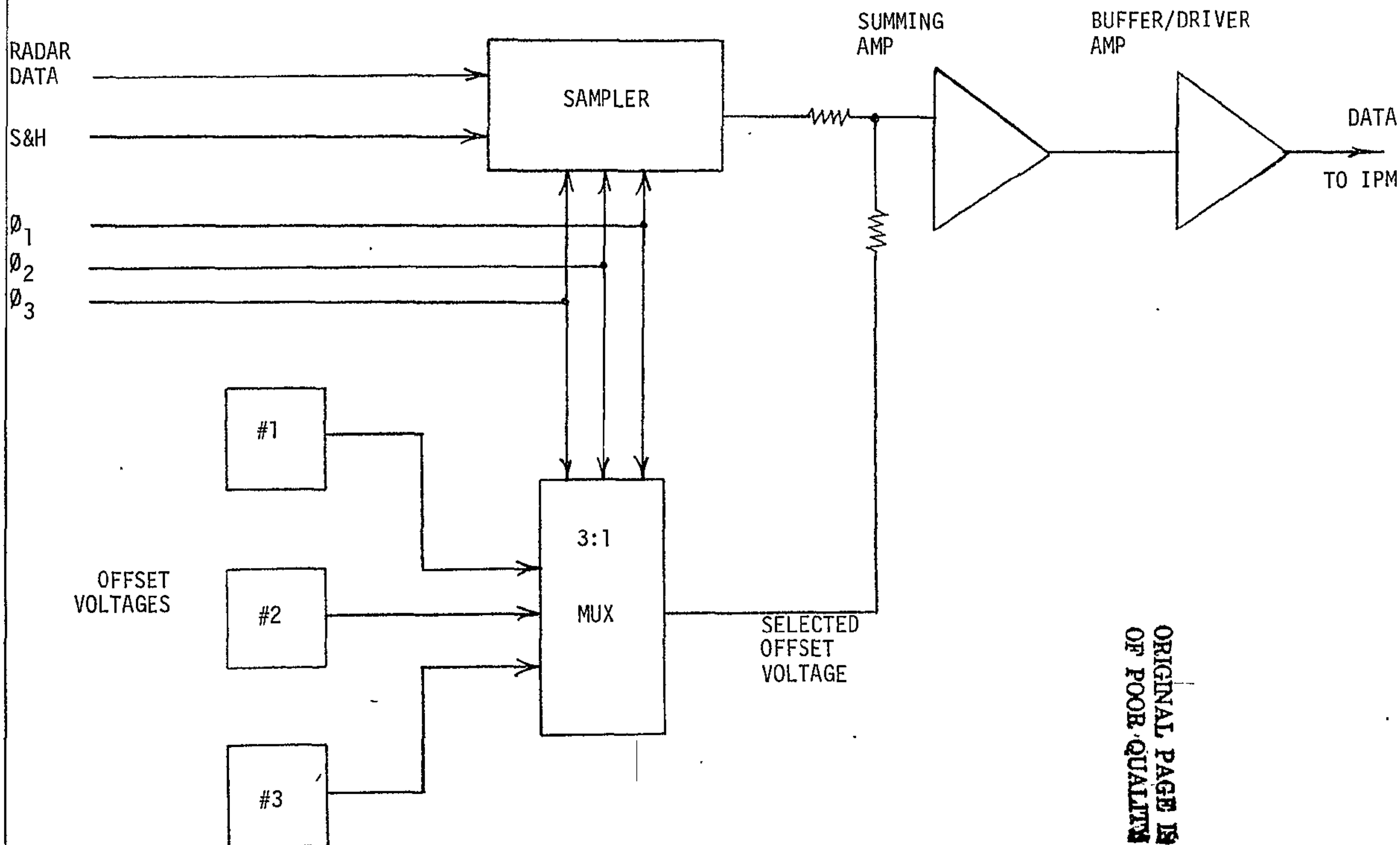

Figure 3-1. Block Diagram of Modulo-3 Correction Circuit

ORIGINAL PAGE IS
OF POOR QUALITY

ground return. Typically, the ground return is an order of magnitude higher in amplitude than the areas of interest. For this reason, the actual processable data had a low amplitude. Typical signal amplitudes were only 5 to 10 percent of the available sampler dynamic range. The return signals were, in most cases, lower in amplitude than the modulo-3 noise present in the sampler output.

Attempts were made to remove modulo-3 noise from the Marineland data using the 960A computer. The attempts were not successful. Scanned tapes of Marineland data were made by JPL from the optically processed flight film. There were mismatches in scan parameters with respect to the Phase III software simulation. However, a poor but recognizable image was produced by the simulation. At that time, the IPM could not be exercised from a 9 track tape. Scanned tapes were useless for IPM checkout until a recent modification to the computer test set was made and additional software written.

2. Ames (August 1976) Flight

The intent for the Ames flight and subsequent flights in August 1976 was to fly the IPM which was to have been checked out using the data gathered during the Marineland (December 1975) flights. The checkout data was not available for reasons outlined in the previous section. This had little impact on the schedule, however, because the IPM checkout was not complete in time for the August 1976 flights. For that reason, it was decided to fly the same equipment as had been flown on the Marineland flights. The problems uncovered then were identified and fixed for the Ames flight.

The sampler (with modulo-3 correction circuitry) and the magnetic tape recorder were flown during the Ames flight (17 August, 1976). The data gathered showed a low level of module-3 noise. The proper time-variable gain video signal was input to the sampler. The appropriate sampler time delays were used. When the Ames data was processed using the software simulation, the image quality was still poor.

Several tests were run to check the Ames data for defects. JPL identified the apparent cause of the poor image quality as a line-to-line synchronization problem in the raw data. After recording the flight data, the digital data is editted and reformatted onto 9 track IBM - compatible magnetic tape. Indications of the synchronization problem are based primarily on observations of reformatted raw data.

Two possible sources of the synchronization problem were suspected and investigated: the reformatting process onto 9 track tape and the sampling process. The entire system was exercised by recording fixed test signals from the sampler test set onto the Sangamo magnetic tape recorder. This test tape was reproduced, reformatted onto 9 track tape and displayed. There was no indication, whatever, of any synchronization problem with the test data. The data patterns were in good registration on all the data checked. The sampler and magnetic tape recorder both function as intended in the lab environment. Since the sampler test set simulates all three radar input signals to the sampler, the only difference between the flight environment and the lab environment is the source of those three signals. A synchronization problem of the kind indicated is difficult to detect in the flight environment since the peak-to-peak jitter is less than 1% (150-200 nanoseconds). Since the radar return appears to be a randomly varying signal with the exception of the ground return and the sampler pedestal, the only hope of identifying the source of the jitter is to use a 9 track tape which contains both a ground return and a sampler pedestal. This was done with data from Goldfield run #4. Displaying successive records showed that the ground returns had the jitter problem identified by JPL. However, the sampler pedestal present on the reformatted data was in good registration from record to record. The significance of this is the fact that the sampler pedestal is inserted into the data stream during the sampling process and is used to trigger the digitizing process. If the ground return jitters but the sampler pedestal does not then the sampling synchronization must be the source of the jitter. If the source of the jitter is the digitizing or reformatting process, then the two signals should both jitter. Synchronization of the sampler to the PRF signal is the most likely candidate for the jitter source. The PRF signal is enabled only when the JPL radar is turned on in flight onboard the CV990 aircraft. This means that to verify or disprove this theory it would be necessary to fly the sampler and magnetic tape recorder again - which is beyond the scope of the program.

Two reformatted 9 track tapes containing a ground return were manipulated by JPL to remove the line-to-line jitter from the data. These tapes were processed using the software simulation and the IPM. Results appeared to be slightly improved but still of poor quality. The two deskewed 9 track tapes represent the only actual sampler radar data obtained from the Ames flights that was of any use for testing.

B. SOFTWARE TESTS

The software tests include two different levels of tests for IPM checkout: subsystem tests and system tests. Subsystem tests are intended to provide test signals for discrete sections of the IPM such as range or azimuth filters. The system tests provide test signals to checkout the IPM and real time display as a complete unit.

1. Subsystem Tests

The key tests to be done at the subsystem level are concerned with the range and azimuth filters. The computer test set provides test waveforms to those filters to measure correlation peak and side lobes. A key measurement for both range and azimuth filters is their combined output phase sensitivity. Ideally, the combined output amplitudes should not be sensitive to input signal phase. This parameter in particular will be measured. The phase shift and cutoff frequency of the presum filter will be measured.

2. System Tests

The system test plans are to provide a parallel processing path that can be used as a benchmark to evaluate the IPM processing. In addition, system level test patterns such as point targets may be used to check the IPM. The software system simulation allows the IPM parameters to be varied and their effects evaluated without hardware changes. This software system simulation is done using a Texas Instruments 960A minicomputer. This simulation was originally done on the Phase II portion of this contract and was subsequently modified and expanded for use on Phase III.

SECTION IV.
TEST RESULTS

A. EQUIPMENT

1. Sampler

The sampler performs the function of sampling and time-expanding the radar return video data. The primary measurements to be made on the sampler are voltage transfer function and noise characterization.

The voltage transfer function defines the output voltage in terms of the input voltage. An input signal (similar to Figure 4-1) is input to the sampler and the output (similar to Figure 4-2) is observed and measured. A graph of the results is shown in Figure 4-3.

The primary noise component in the sampler input is modulo 3 noise. A typical sampler output for a zero input and no modulo-3 correction is shown in in Figure 4-4. The best modulo 3 correction achievable for a zero input is shown in Figure 4-5. Modulo 3 noise is due to a gain imbalance between the three parallel CCD shift registers. Modulo 3 noise amplitude will be directly proportional to input voltage unless corrected. The correction circuitry attempts to compensate for this gain function with fixed offset voltages. For this reason, the voltage range of the best correction will be limited. A graph of modulo 3 noise amplitude versus input voltage is shown in Figure 4-6.

2. IPM

a. Range and Azimuth Filters: The basic operation of the range and azimuth filters is similar. The tap weights of the CCD transversal filters are different as shown in Tables 2-2 and 2-3. The filters are clocked at different rates; range at 543 KHz and azimuth at 1.1 MHz. The test scheme consists primarily of inputting chirp waveforms generated by the computer test set and measuring the correlation peak. Examples of range filter waveforms are shown in Figure 4-6. Examples of azimuth filter waveforms are shown in Figure 4-7.

The phase of the input signal is continuously varying. Ideally, the sum of the squared outputs of the real and imaginary components of both filters should be independent of input phase. The degree to which this is true is a measure of the gain imbalance between the real and imaginary components.

A test of phase sensitivity was run on both the range and azimuth filters. The range filter phase sensitivity is shown in Figure 4-8. The azimuth filter phase sensitivity is shown in Figure 4-9. These phase sensitivity

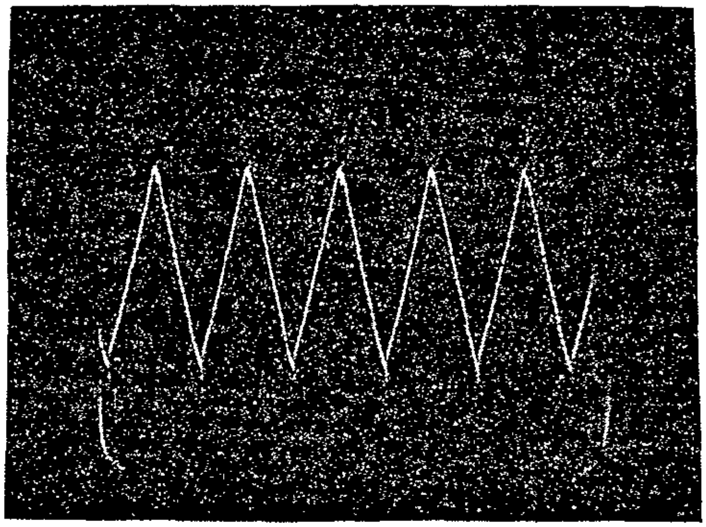

1ms/div

200 mv/div

Figure 4-1. Sampler Input
(From Test Set)

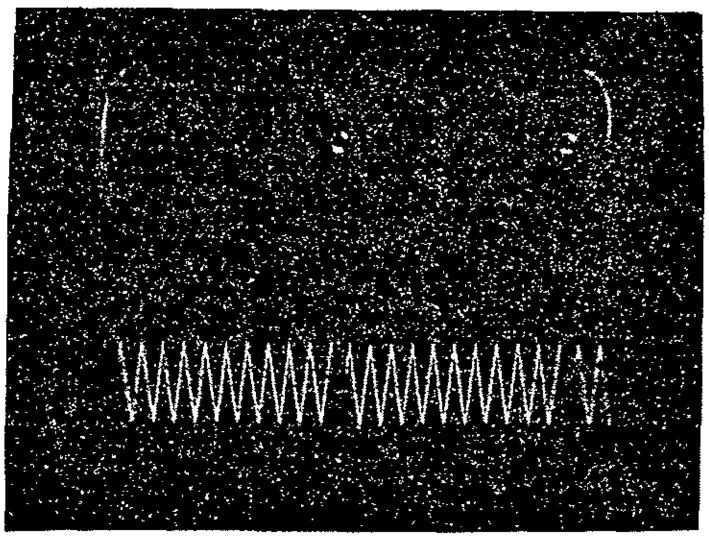

0.2 ms/div

1v/div

Figure 4-2. Sampler Output
to Magnetic Tape Recorder

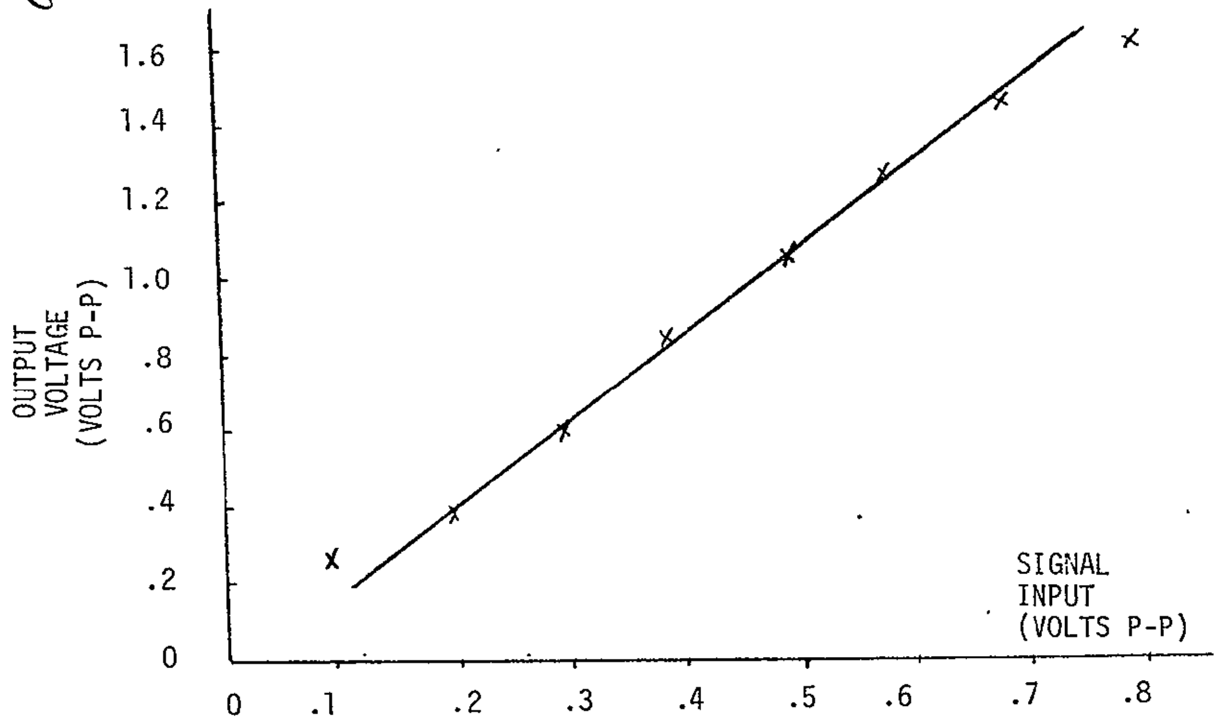

Figure 4-3a. Sampler Voltage Transfer Function

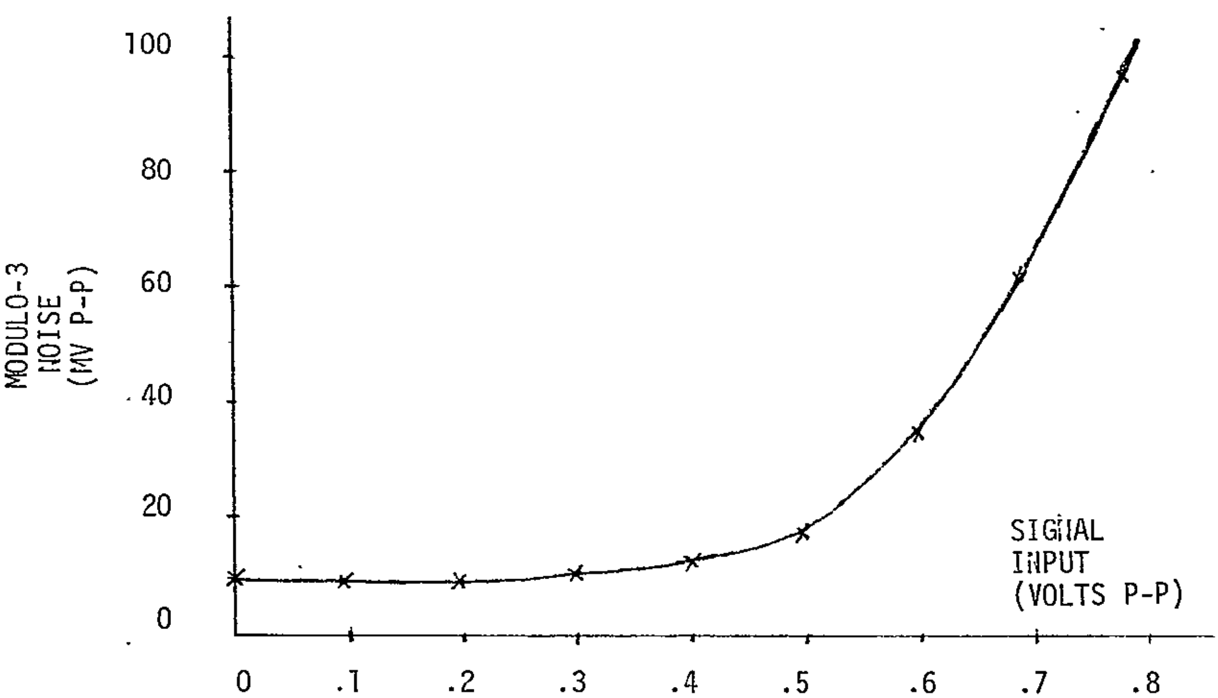

Figure 4-3b. Modulo-3 Noise vs Input Signal Level

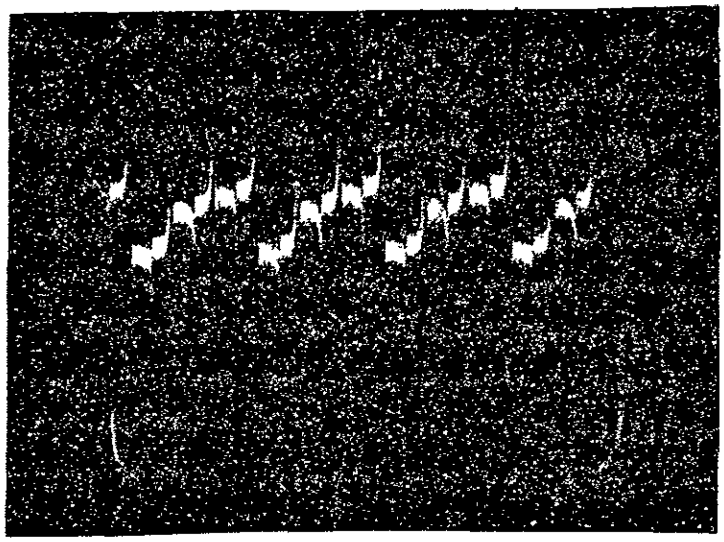

Figure 4-4. Sampler Output Without Modulo 3 Correction

ORIGINAL PAGE IS OF POOR QUALITY

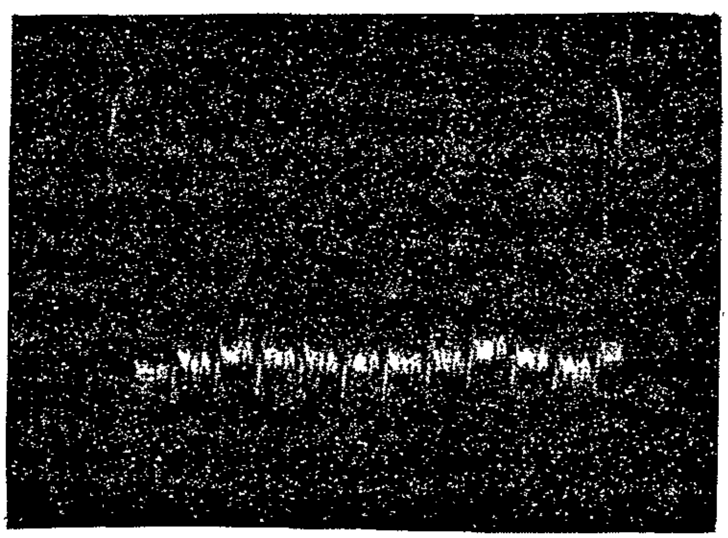

Figure 4-5. Sampler Output With Modulo 3 Correction

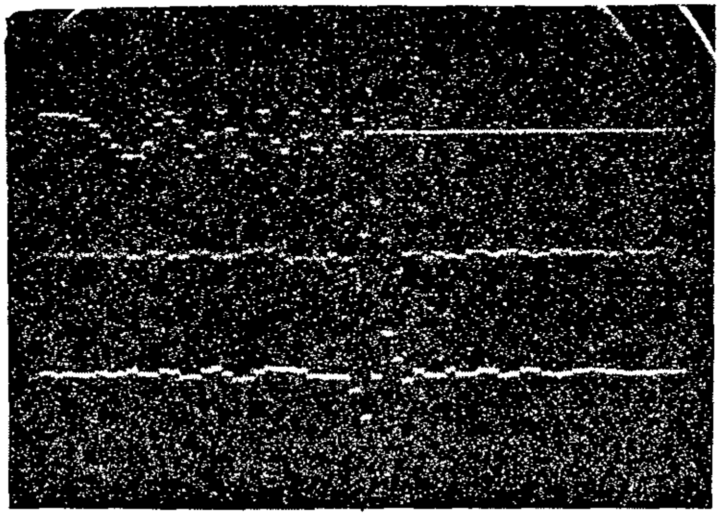

Input
(5V/div

I Output
(2V/div)

Q Output
(2V/div)

20 μs/div →

0°

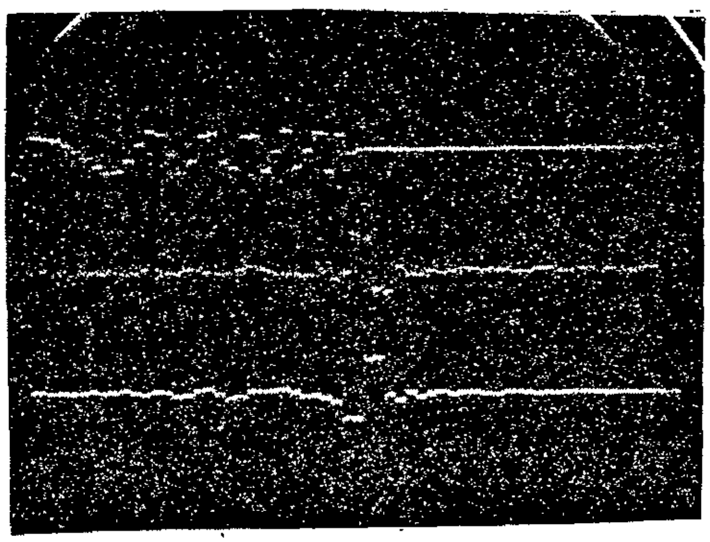

Input
(5V/div)

I Output
(2V/div)

Q Output
(2V/div)

45°

Figure 4-6. Range Filter Waveforms

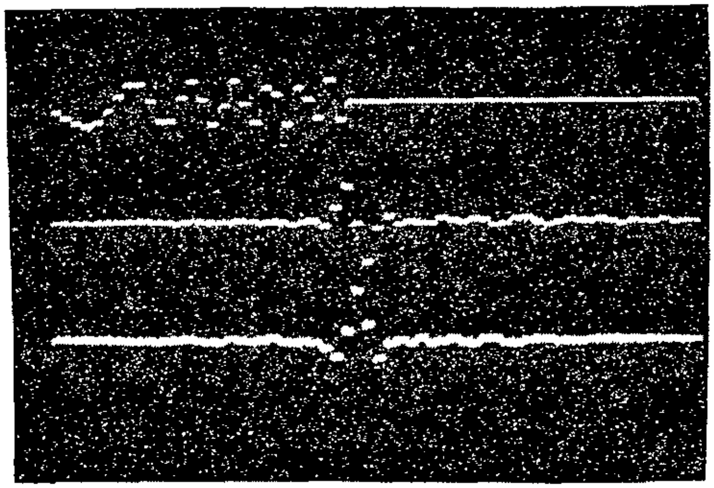

Input
(5V/div)

I Output
(2V/div)

Q Output
(2V/div)

20 μs/div →

90°

ORIGINAL PAGE IS
OF POOR QUALITY

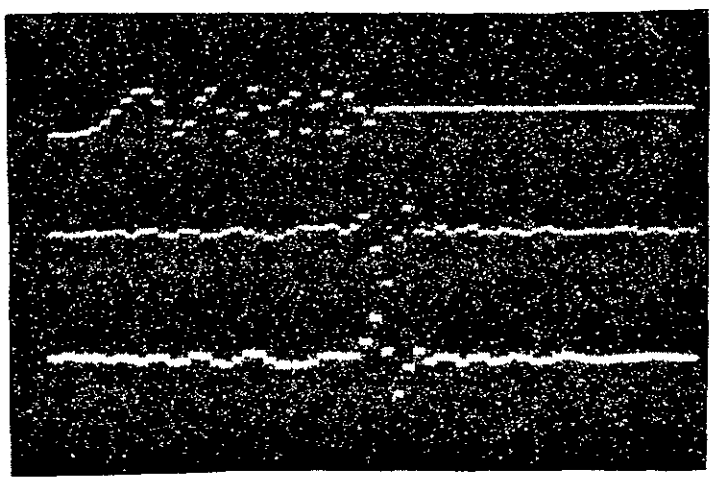

Input
(5V/cm)

I Output
(2V/cm)

Q Output
(2v/cm)

20 μs/div →

180°

Figure 4-6. (Continued)

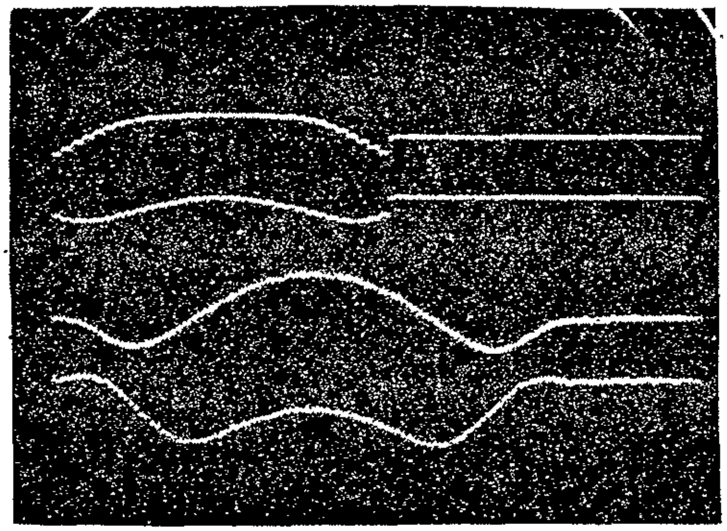

I Input (5V/div)

Q Input (5V/div)

I Output (2V/div)

Q Output (2V/div)

20 µs/div →

0°

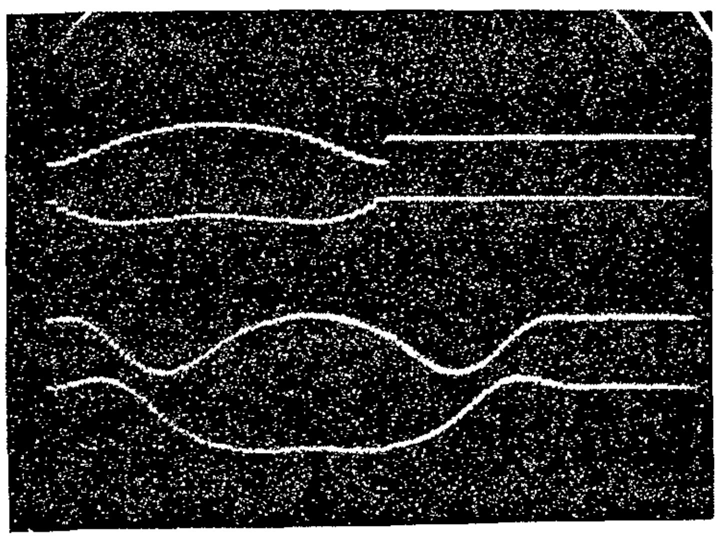

I Input(5V/div)

Q Input(5V/div)

I Output (2V/div)

Q Output (2V/div)

20 µs/div →

45°

Figure 4-7. Azimuth Filter Waveforms

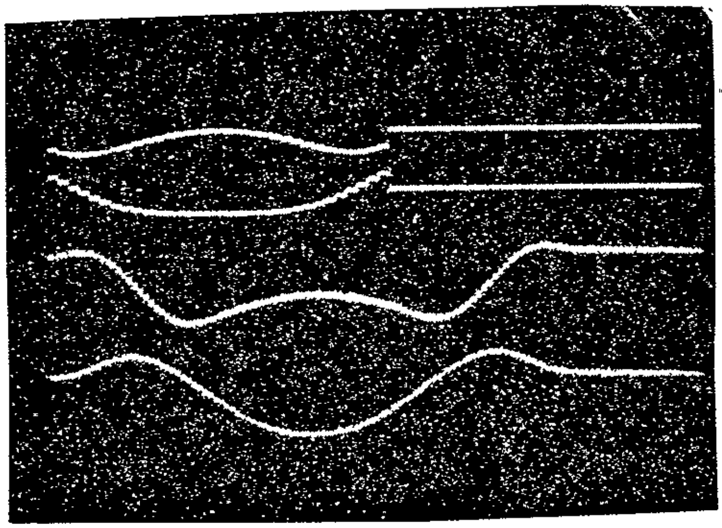

I Input (5V/div)

Q Input (5V/div)

I Output (2V/div)

I Output (2V/div)

20 μs/div

90°

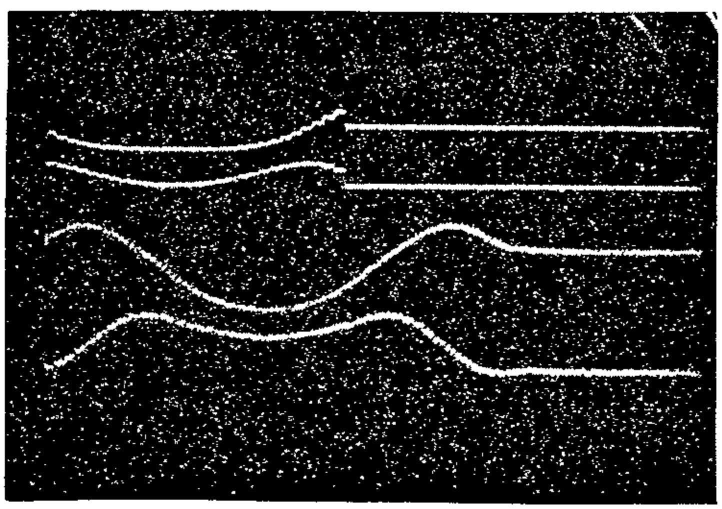

I Input (5V/div)

Q Input (5V/div)

I Output(2V/div)

Q Output(2V/div)

20 μs/div

180°

ORIGINAL PAGE IS
OF POOR QUALITY

Figure 4-7. (Continued)

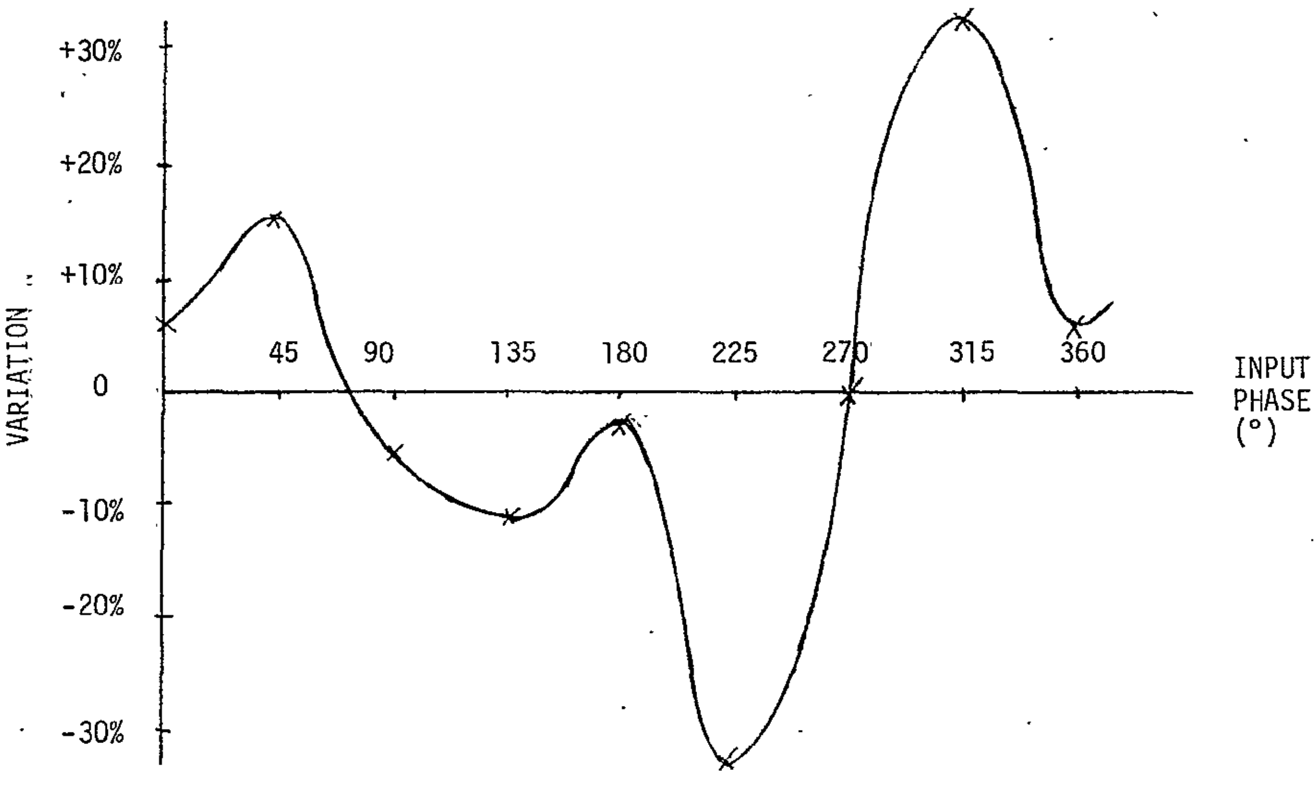

Figure 4-8. Range Filter Phase
Sensitivity

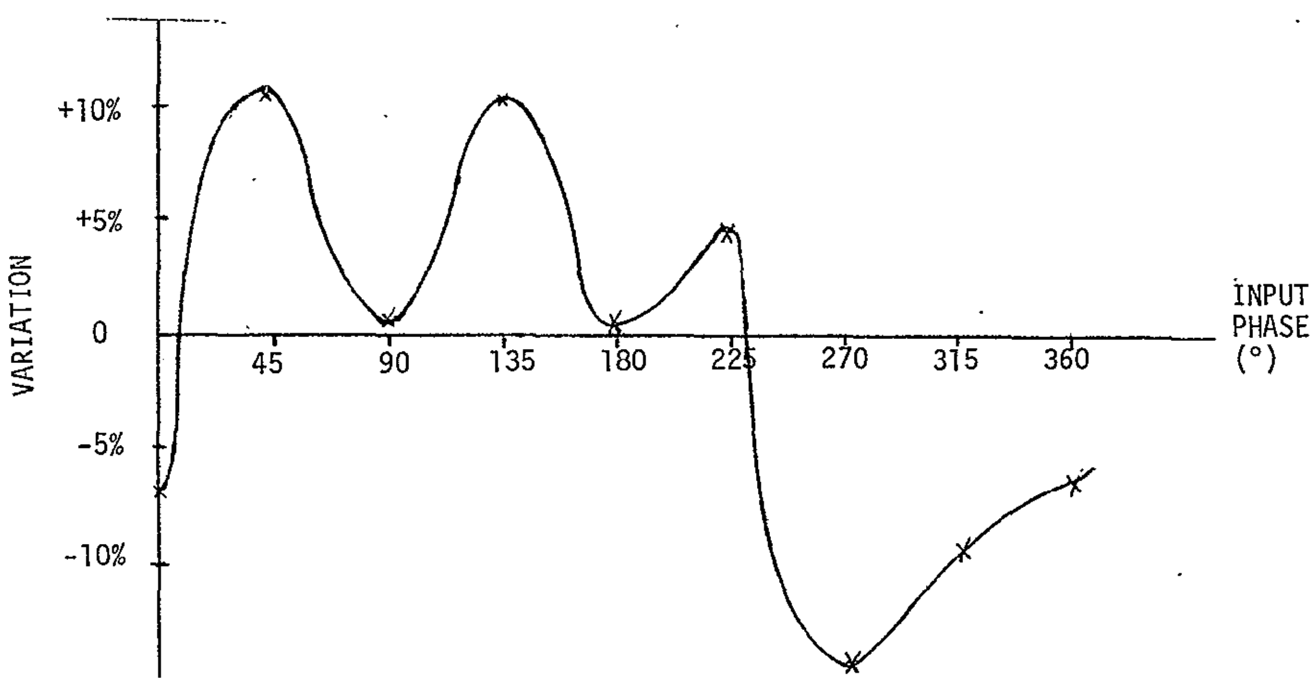

Figure 4-9. Azimuth Filter Phase
Sensitivity

figures were subjected to further investigation and a computer analysis.

The computer analysis of the CCD transversal filters included the simulation of electrode overlap capacitive effects to determine the extent of any errors in the filter response due to average weighting coefficient effects. The circuit shown in Figure 4-10 indicates the equivalent circuit for a CCD transversal filter and associated differential current integrators (DCI). C_{k2}^{+}, C_{k3}^{+}, C_{k4}^{+} represent capacitive coupling between the positive tapped electrode (phase 1^{+}) clock line buss and the phase 2, 3, and 4 clock line busses, respectively. Likewise, C_{k2}^{-}, C_{k3}^{-}, and C_{k4}^{-} represent capacitive coupling between the negative tapped electrode (phase 1^{-}) clockline buss and phase 2, 3, and 4 clock line busses. C_{OL2} and C_{OL4} indicate the capacitive coupling between the tapped electrodes and the phase 2 and 4 clock electrodes. The transfer of charge under the tapped electrodes is modeled by the application of a voltage V_i at the junction of the electrode oxide capacitance C_e and the depletion capacitance C_D. $C_s^{\pm}$ represents the stray capacitance along the tapped electrode clock line busses, and C_I is the integration capacitance of the DCI. During the time ϕ_1 is off the integrating capacitors are charged to V_{ref} and the ϕ_1 busses are clamped to ground. When ϕ_1 turns on, the clamps to V_{ref} are removed and the two lines connected together resulting in the redistribution of charge. The voltage across the busses may now be calculated using superposition to be:

$$V_F^{\pm} = \frac{C_I V_{ref}}{C_\Sigma^{\pm}} + \frac{V_2 C_{k2}^{\pm}}{C_\Sigma^{\pm}} + \frac{V_3 C_{k3}^{\pm}}{C_\Sigma^{\pm}} + \frac{V_4 C_{k4}^{\pm}}{C_\Sigma^{\pm}} + \frac{V_2 \Sigma (1 \pm h_i) C_{OL2}}{2C_\Sigma^{\pm}} +$$

$$\frac{V_4 \Sigma (1 \pm h_i) C_{OL4}}{C_\Sigma^{\pm}} + \frac{\Sigma V_i (1 \pm h_i) C_e}{2C_\Sigma^{\pm}} \tag{4-1}$$

where $$C_\Sigma^{\pm} = C_I + C_s^{\pm} + N(C_{k2}^{\pm} + C_{k3}^{\pm} + C_{k4}^{\pm}) + \frac{N(1 \pm h^{-})}{2} (C_{OL2} + C_{OL4} + C_e) \tag{4-2}$$

where $$h^{-} = \frac{\sum_{i=1}^{N} h_i}{N} \tag{4-3}$$

the voltage V_i may be further defined as

ORIGINAL PAGE IS OF POOR QUALITY

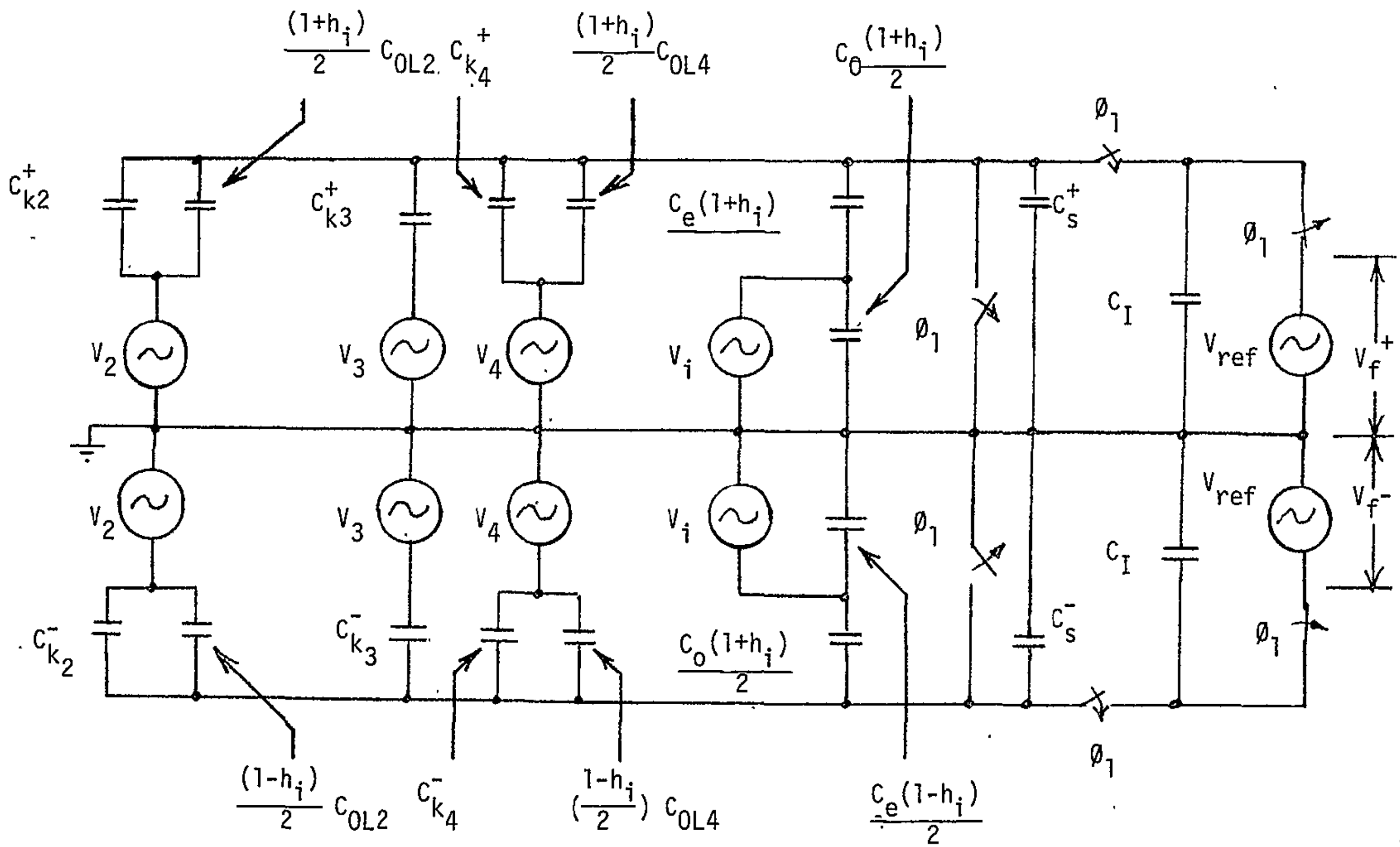

FIGURE 4-10.
SCHEMATIC REPRESENTATION OF CCD TRANSVERSAL
FILTER AND DIFFERENTIAL CURRENT INTEGRATOR

$$V_i = V_z + V_{sig_i} \qquad (4\text{-}4)$$

where V_z is a dc offset or "fat zero" voltage and V_{sig_i} is the signal voltage present in the i^{th} stage. Differencing the voltage on the two busses gives:

$$V_o = V_F^+ - V_F^- = C_I V_{ref} \left[\frac{1}{C_\Sigma^+} - \frac{1}{C_\Sigma^-}\right] + V_2\left[\frac{C_{k2}}{C_\Sigma^+} - \frac{C_{k2}}{C_\Sigma^-}\right] + V_3\left[\frac{C_{k3}}{C_s^+} - \frac{C_{k3}}{C_s^-}\right] +$$

$$V_4 \left[\frac{C_{k4}^+}{C_\Sigma^+} - \frac{C_{k4}^-}{C_\Sigma^-}\right] + \frac{V_2 C_{OL2} + V_4 C_{OL4} + V_z C_e}{2} \left[\frac{\Sigma(1+h_i)}{C_\Sigma^+} - \frac{\Sigma(1-h_i)}{C_\Sigma^-}\right] +$$

$$\frac{C_e}{2} \left[\frac{\Sigma V_{sig_i}(1+h_i)}{C_s^+} - \frac{\Sigma V_{sig_i}(1-h_i)}{C_s^-}\right] \qquad (4\text{-}5)$$

To calculate all of the on-chip capacitive constants in equation 5, measurement of all clockline overlap areas were made from the original drawings of the CCD transversal filters. Once the overlap dimensions were obtained, the overlap capacitances were calculated using the interlevel capacitive characteristics of the single level polysilicon process used in the production of the CCD's. The calculated values of all overlap capacitances for the IPM CCD filters are shown in Table 4-1.

In the computer simulation, $\emptyset_2$ is assumed to be ON during the charge sensing interval ($\emptyset_1$ ON). $\emptyset_3$ and $\emptyset_4$ are assumed to be OFF during this interval ($V_3 = V_4 = 0$) so equation 4 simplifies to

$$V_o = C_I V_{ref} \left(\frac{1}{C_\Sigma^+} - \frac{1}{C_\Sigma^-}\right) + V_2\left(\frac{C_{k2}^+}{C_\Sigma^+} - \frac{C_{k2}^-}{C_\Sigma^-}\right) + \frac{V_2 C_{OL2} \pm V_z C_e}{2}$$

$$\left[\frac{\Sigma(1+h_i)}{C_\Sigma^+} \; \frac{\Sigma(1-h_i)}{C_\Sigma^-}\right] + \frac{C_e}{2} \left[\frac{\Sigma V_{sig_i}}{C_\Sigma^+} - \frac{\Sigma V_{sig_i}(1-h_i)}{C_\Sigma^-}\right] \qquad (4\text{-}6)$$

This expression contains contributions from dc components and signal average value components in addition to the desired component. In general, this expression cannot be significantly simplified unless the average value of the filter weighting coefficients is zero.

Table 4-1
Overlap Capacitances for CCD Filters

$C_{k2}^{+} = .0014$ pf	$C_{k2}^{-} = .0299$ pf	$C_{OL2} = .0408$ pf
$C_{k3}^{+} = 0$	$C_{k3}^{-} = .0245$ pf	$C_{OL4} = .0408$ pf
$C_{14}^{+} = .0299$ pf	$C_{k4}^{-} = .0014$ pf	$C_{e} = .0924$ pf
$C_{s}^{+} = 1.331$ pf	$C_{s}^{-} = 1.784$ pf	

The computer analysis of the CCD transversal filters also included the simulation of charge transfer efficiency (CTE) effects. $V_{sig(i,n)}$ represents the voltage produced by a charge packet under the i^{th} tapped electrode of the CCD transversal filter after the n^{th} transfer of charge down the CCD channel. Upon application of the four phase clocks, the charge packet is transferred under the $i^{th}+1$ tapped electrode. Due to charge transfer inefficiency the voltage produced by the charge packet is given by:

$$V_{sig(i+1,\ n+1)} = \alpha V_{sig(i,n)} + \beta V_{sig(i+1,n)} \tag{4-7}$$

where $\alpha = \eta^4$ and $\beta = 1-\alpha$

and η is the actual CTE of the CCD filter.

The input signals to the CCD filters in the computer simulation were derived to simulate the desired matched filter conditions. For the range filters, which have Dolph Chebyshev weighted filter tap weights, the same input samples were applied to both the cosine and sine filters. The i^{th} input sample is given by

$$V_{in(i)} = C[(\cos\emptyset)\ h_c\ (N+1-i) - (\sin\emptyset)\ h_s\ (N+1-i)] \tag{4-8}$$

where $h_{c(i)}$ is the i^{th} range cosine unweighted tape weight

$h_{s(i)}$ is the i^{th} range sine unweighted tap weight

$\emptyset$ is the phase angle of the input signal

C is a magnitude scaling constant

N is the number of filter taps

ORIGINAL PAGE IS OF POOR QUALITY

The azimuth filters also have Dolph-Chebyshev weighted tap weights. In phase and quadrature signal samples were applied to both the sine and cosine azimuth filters. The in-phase signal component is given by

$$V_{ini(i)} = C\ [(\cos\emptyset)\ h_c\ (N+1-i) - (\sin\emptyset)\ h_s(N+1-i)] \tag{4-9}$$

The quadrature component is given by

$$V_{ing(i)} = C[(\sin\emptyset)\ h_c\ (N+1-i) + (\cos\emptyset)\ h_s\ (N+1-i)] \tag{4-10}$$

The outputs of the azimuth cosine and sine filters were summed and squared for both the I and Q channels. The squared I and Q outputs are then combined to complete the complex convolution operation. The final azimuth filter output is given by

$$V_{out} = \sqrt{(RxR + IxI)^2 + (RxI - IxR)^2} \tag{4-11}$$

where RxR is the output of the azimuth cosine filter with in-phase input. IxR is the output of the azimuth cosine filter with quadrature input. IxI is the output of the azimuth sine filter with quadrature input. RxI is the output of the azimuth sine filter with in-phase input.

It was found that the range filters are not phase invariant. Figure 4-11 shows the computed phase variance of the range filters in the ideal case of a CCD filter with capacitive imbalances and no charge transfer inefficiency. The amplitude of the matched filter response varies more than $\pm 10\%$ of the average amplitude for varying input signal phase and constant input signal magnitude. This result would indicate that the major contribution to the phase variance of the range filters originates with the filter coefficients which are Dolph-Chebyshev weighted and produce a truncated chirp impulse response. Figure 4-11 also shows the phase variance of the range filters obtained by a full implementation of the CCD filter model. The results show a slightly increased phase variation, due to the capacitive imbalances caused by nonzero average range filter coefficients.

Due to the highly oversampled chirp function used to calculate the tap weights for the azimuth filters, the average tap weight values were increased by approximately an order of magnitude over those existing in the range filters. This increases the magnitude of the signal average value error term of equation 4-6

$$V_{error} = \frac{C_e}{2} \left(\frac{1}{C_\Sigma^+} - \frac{1}{C_\Sigma^-}\right) \Sigma V_{sig_i} + \text{dc terms} \tag{4-12}$$

Neglecting the dc terms, the magnitude of this error is less than 1.5 percent of the output signal magnitude in all four azimuth filters,

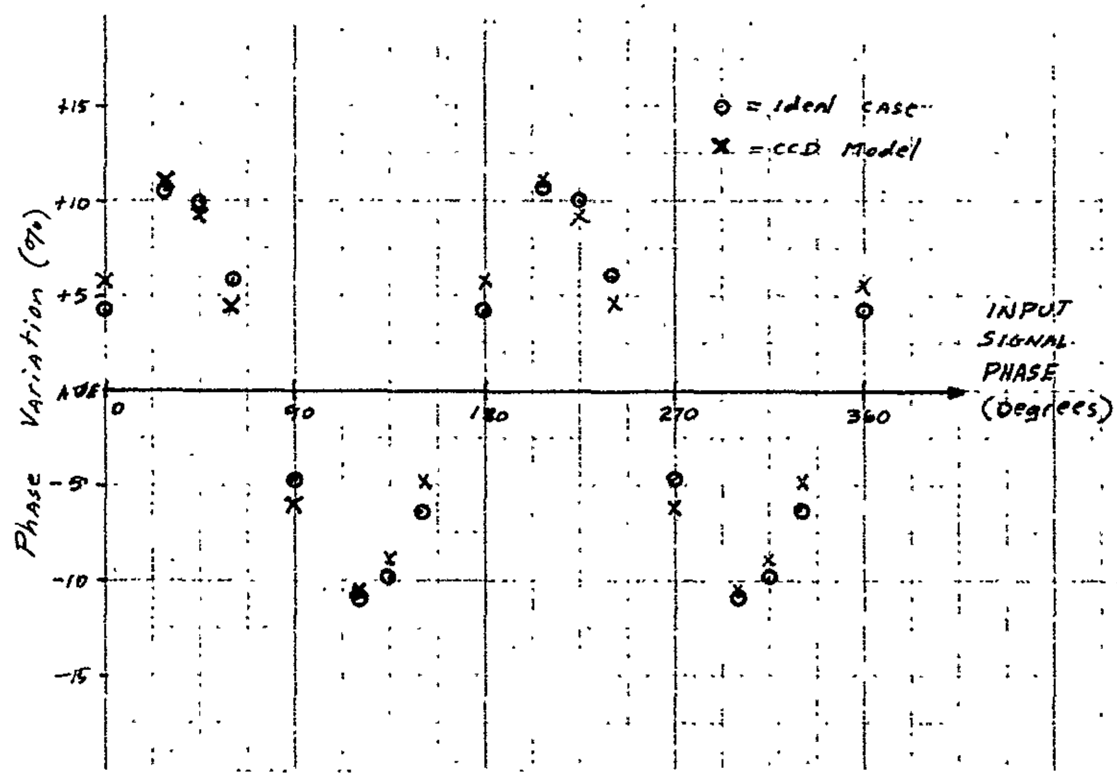

Figure 4-11. Range Filter Phase Variation

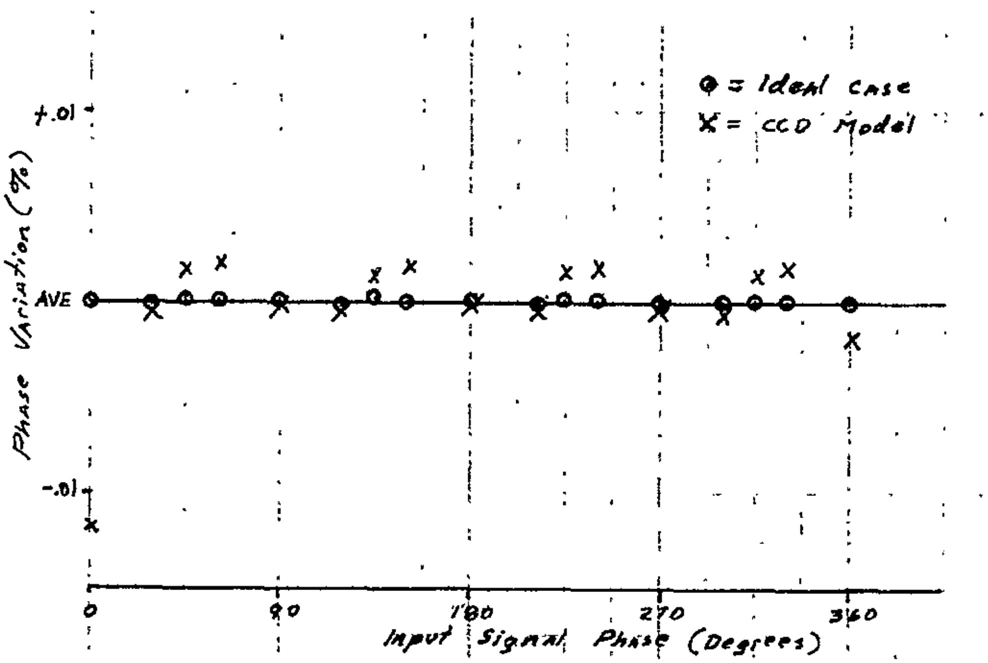

ORIGINAL PAGE IS OF POOR QUALITY

Figure 4-12. Azimuth Filter Phase Variation resulting in less than a 2.5 percent error in final output magnitude after the in phase and quadrature outputs have been summed and squared. This error is phase invariant at the output. The unweighted azimuth tap weight values produce a nearly phase invariant matched filter response, and the complete CCD filter simulation of the azimuth system produced a phase variance of less than 0.1 percent of total output magnitude at the correlation peak. The phase variance of the azimuth filter is shown in Figure 4-12.

In all cases, dc error terms due to clock line overlap and the integration capacitor precharge were the dominant terms in the CCD filter error analysis. These terms contributed dc errors that in general were at least an order of magnitude greater than the peak output signal magnitude. All dc errors can be compensated by accurate ac coupling at the outputs of the CCD transversal filters.

The accuracy of the ac coupling operation before the CCD azimuth outputs are summed and squared could be a dominating factor in the creation of false sidelobes in the correlation process. Any negative offsets created by the integration effect of the ac coupling capacitors would result in positive sidelobes after the squaring operation. The magnitude of these false sidelobes would depend on the waveshape of the CCD filter output signals, which in turn is dependant on the type of input signal that is to be processed.

Other than the inherent phase variation of the CCD range filters, it was found that all second order effects of the CCD filter implementation are negligible in the pulse compression system. Average value tap weight error terms and CTE effects both have very slight effect on the matched filter correlation peak magnitude. This analysis does not take into account any inaccuracies due to the processing system that exists off the CCD transversal filter chip. No consideration was given to stray capacitances in the signal path on the PC boards of the processor, nor did this analysis account for any DCI errors such as integration capacitor mismatches.

b. Presum Filter and Azimuth Memories

The presum filter is a low pass, 2 pole, Butterworth filter with a 10 Hz cutoff frequency. The presum filter is implemented digitally and multiplexed between the I and Q channels. Appendix A shows the basis for the digital (powers of two) filter implementation. A functional block diagram of the presum filter and azimuth memory section is shown in Figure 2-9. Presum filtering allows a reduction in the data rate by a factor of 8.

The azimuth memories are two 8K x 8 MOS random access memories. A block diagram of the azimuth memory section is shown in Figure 2-11. The azimuth memories contain 32 successive range lines of 240 samples each. The range lines are loaded into memory as they are collected from the presum filter. The memory performs a "corner-turning" function by unloading the data by range sample for all 32 samples in chronological order.

The presum filters and azimuth memories were tested by measuring the magnitude and phase of their frequency response. A sine wave generator which can be synchronized to the PRF signal and varied in frequency from dc to 40 Hz was used. The test signal was sampled at 271 KHz and input to the IPM analog-to-digital converters. The digitized sine wave signal was applied to the presum filter. The resulting output sine wave signal was observed both at the output of the presum filters and at the azimuth memories outputs (via DAC's built in for this purpose).

The frequency response for the presum filter is shown in Figure 4-13. The phase shift is shown in Figure 4-14. The corner frequency actually measured was in the neighborhood of 7 Hz instead of 10 Hz. This difference was not considered to be a problem. The difference is due primarily to the approximations inherent in the digital implementation. The frequency and phase shift of the presum filter output is preserved through the azimuth memories. No separate data was taken for the azimuth memories. In addition, since the presum filter is multiplexed between I and Q channels, the outputs of I and Q channels will be identical given identical inputs. For this reason, only one plot is shown for both channels.

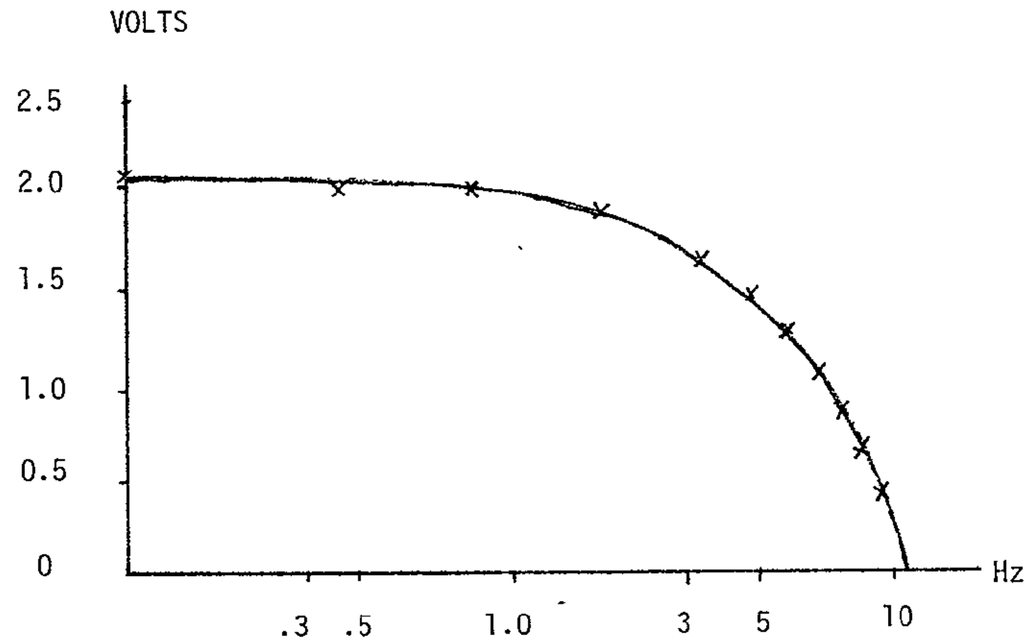

Figure 4-13. Presum Filter Frequency Response

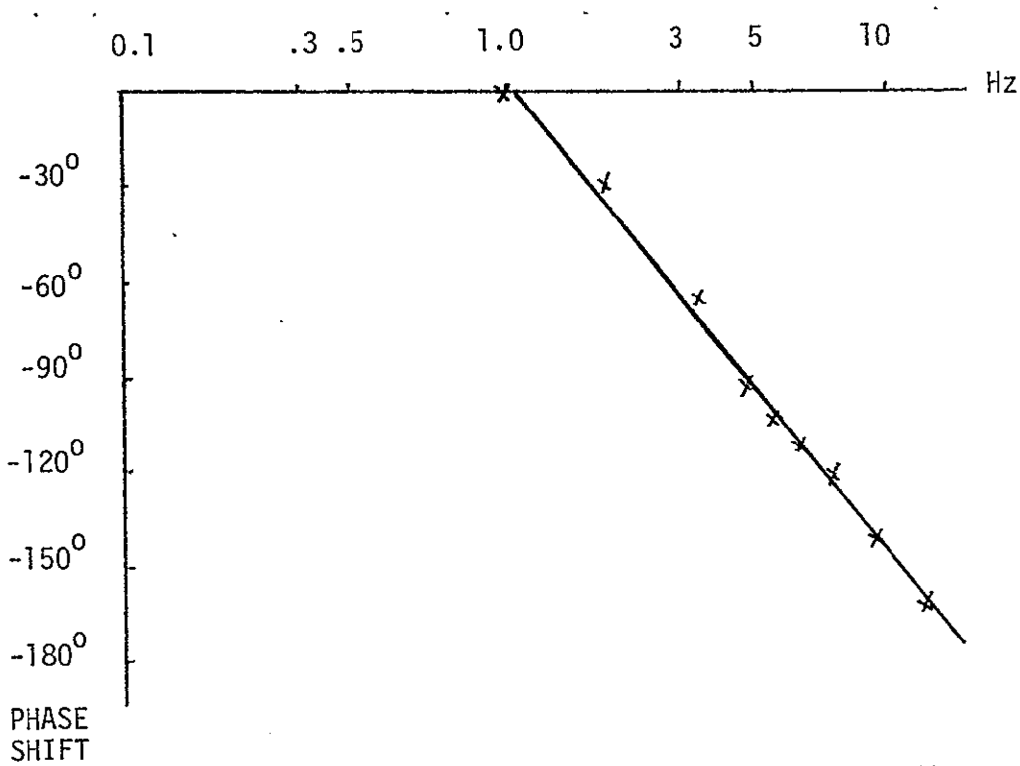

Figure 4-14. Presum Filter Phase Shift vs. Frequency

c. Magnituding Circuitry

Both static and dynamic tests were used to test the magnituding circuitry. The magnituding circuitry is shown in the IPM block diagram (Figure 2-6). The digital squaring circuit is implemented using a programmable read-only memory (PROM) lookup table. This circuit was tested statistically by comparing output bit patterns to jumpered input bit patterns. The magnituding circuitry was tested dynamically by putting test signals from the IPM test set into the magnituding circuit's sample and hold. The IPM output is connected to a DAC for observation purposes.

Triangular wave inputs give hyperbolic outputs and square wave inputs give square wave outputs etc.

3. Real Time Display

The real time display consists of a digital scan converter, a standard TV monitor and an input interface. A built in test pattern generator is used to test the digital scan converter and display. Once this is operating, the entire system including the input interface is exercised by one of several input ports. A 9 track magnetic tape containing several standard images (Bell Girl, etc) was supplied by JPL. These images were dumped through the computer test set and output to display. A typical image is shown in Figure 4-15.

B. PROCESSING RESULTS

As soon as the IPM subsystem level tests were completed, the IPM was used to begin processing the Ames flight data. The processed pictures were of poor quality. An example of an IPM processed picture from the Ames flight (Goldfield run #4) is shown in Figure 4-16. An investigation of the cause(s) of the poor image quality followed.

A modification was made to the real-time display to allow presentation of unprocessed radar data. Examination of the data indicated the jitter problem detailed earlier. An example of raw data is shown in Figure 4-17. JPL succeeeded in deskewing a small quantity of raw data. This deskewed data was used for the remainder of the IPM evaluation.

The deskewed data was processed both by the IPM and the software simulation. Both sources yielded images of low contrast and soft focus. A typical software processed image is shown in Figure 4-18. It was decided at this point to use point targets to investigate the processing problems further.

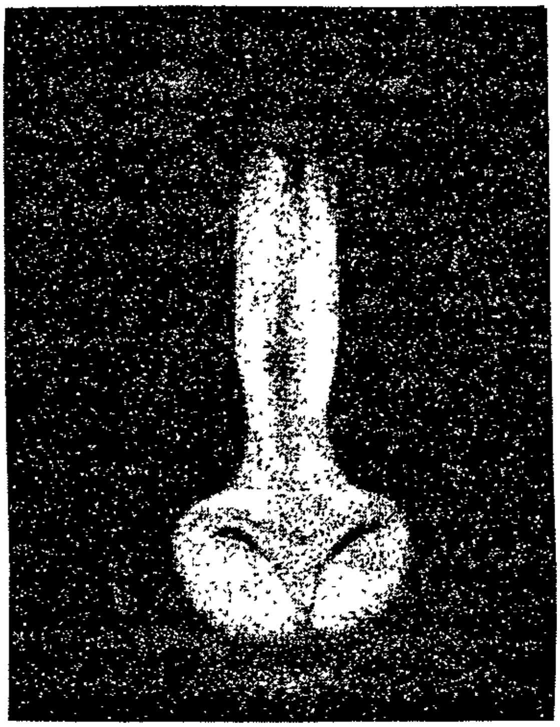

Figure 4-15. Real Time
Display Image (Mandrill)

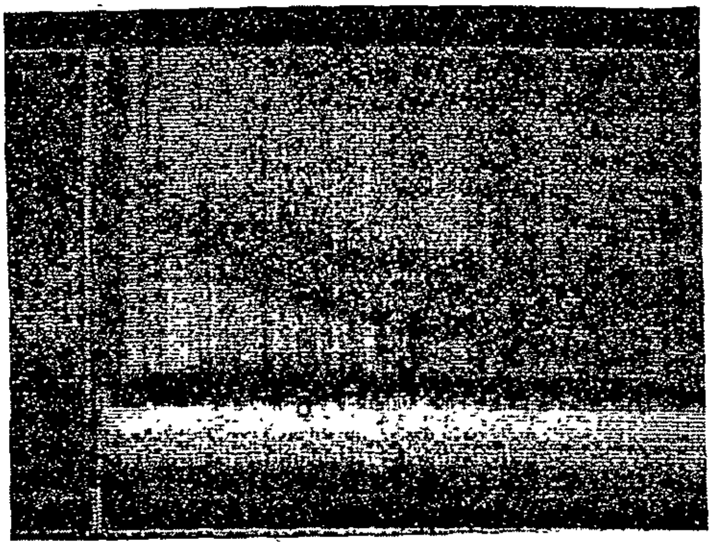

Figure 4-16. IPM Processed Image
(Data From Ames Checkout
Flight-Goldfield Run No. 2)

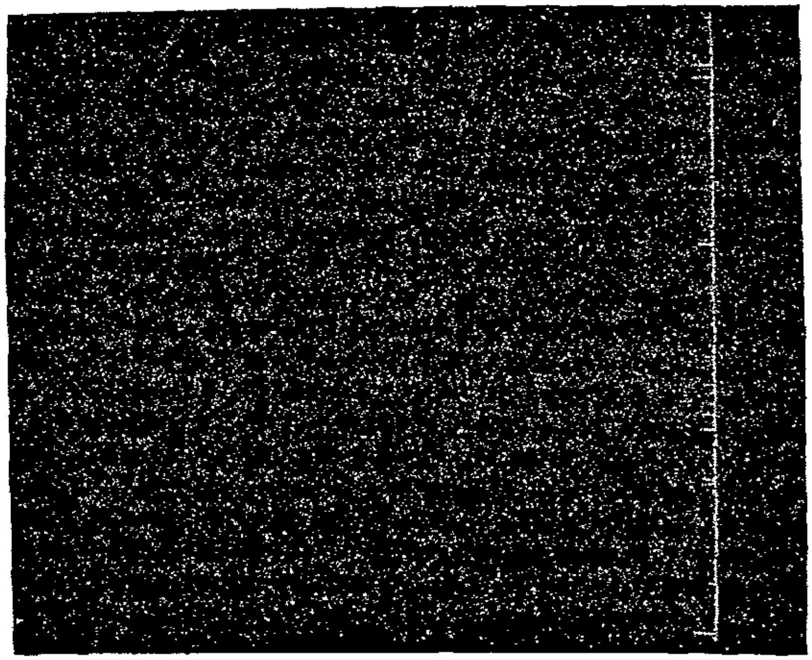

Figure 4-17. Unprocessed Radar Data
(512X512 pixels)

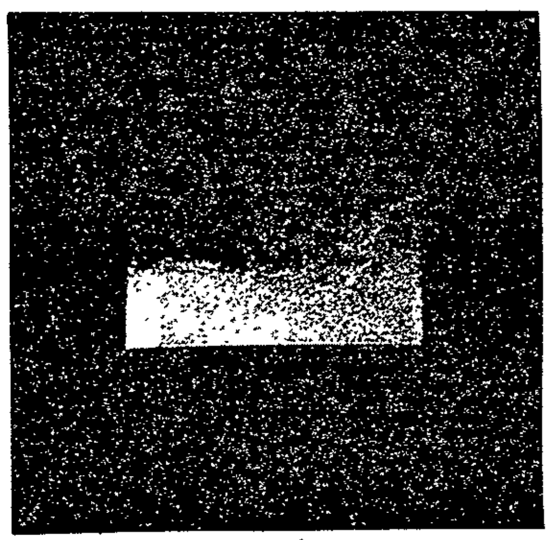

ORIGINAL PAGE IS
OF POOR QUALITY

Figure 4-18. Typical Software Simulation Processed Image (Data From Ames Checkout Flight-Moffet to Goldfield)

Several point target tapes were generated which varied different parameters such as range bin, signal intensity and signal phase. Figure 4-19 and 4-20 show point targets varying in range bin processed by the IPM and software simulation, respectively. Figure 4-21 and 4-22 show point targets varying in input phase, again processed by the IPM and software simulation. Although it is not apparent from the photographs, there was a variation in the intensity and sharpness of the point targets as a function of phase. As previously discussed, this phase sensitivity is felt to be a problem inherent in the CCD filter design. The analysis outlined in the range and azimuth filter sections was conducted to examine this phase sensitivity in greater detail.

In addition to the phase problem, investigation by JPL suggested that a dc offset problem, in either the range or azimuth filters, might be contributing to the poor processed image quality. The weightings of both filters were totalled and each showed a residual dc component. The filter weightings for both range and azimuth were biased in order to minimize the dc offset. The software simulation was modified with the new filter coefficients and an image processed. The new filter coefficients yielded an image with better fine detail, but much higher contrast. Contrast range is in fact too great for the real time display to handle in 16 gray shades. The baseline image is shown in Figure 4-23. The same data processed with the new filter coefficients is shown in Figure 4-24. Tables 4-2 and 4-3 are a listing of the modified filter coefficients. Although further refinement in filter tap weights might have improved the processed picture quality, the program schedule did not permit a continuation of this effort.

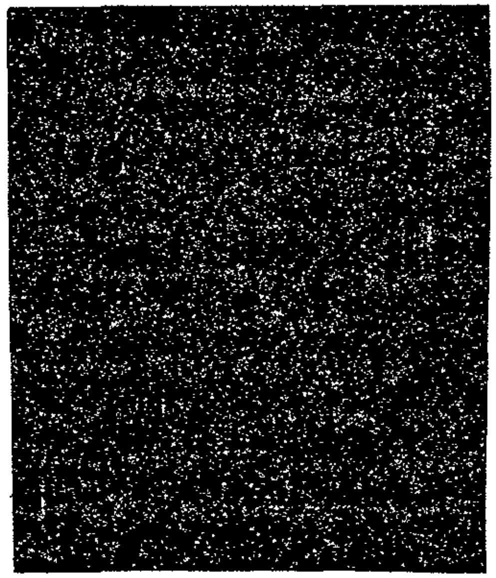

Figure 4-19. IPM Processed Point Targets (Varying in Range Location)

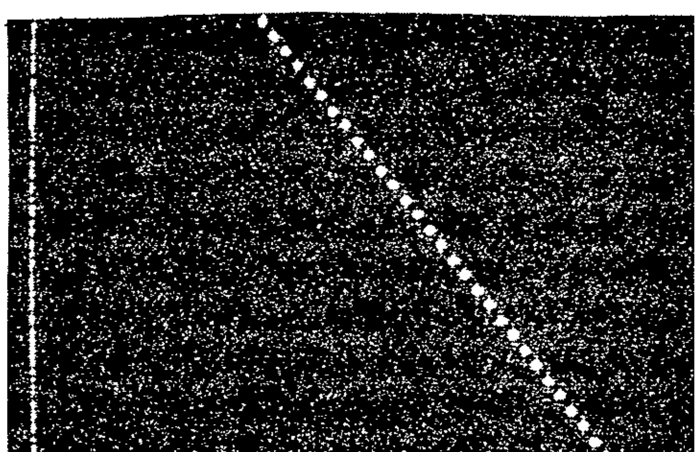

Figure 4-20. Software Processed Point Targets (Varying in Range Location)

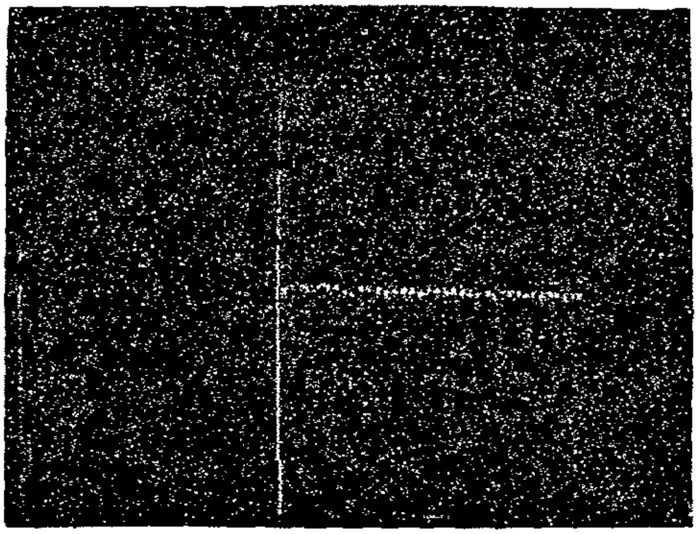

Figure 4-21. IPM Processed Point Targets (Varying Phase in 10 Degree Increments)

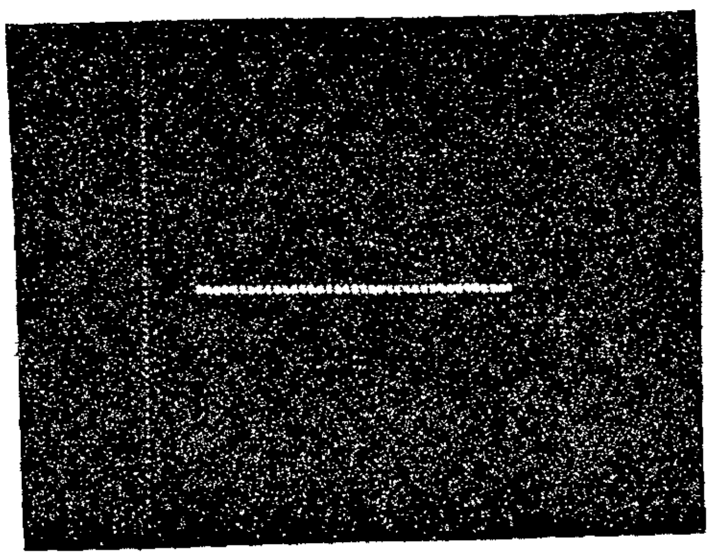

Figure 4-22. Software Processed Point Targets (Varying Phase in 10 Degree Increments)

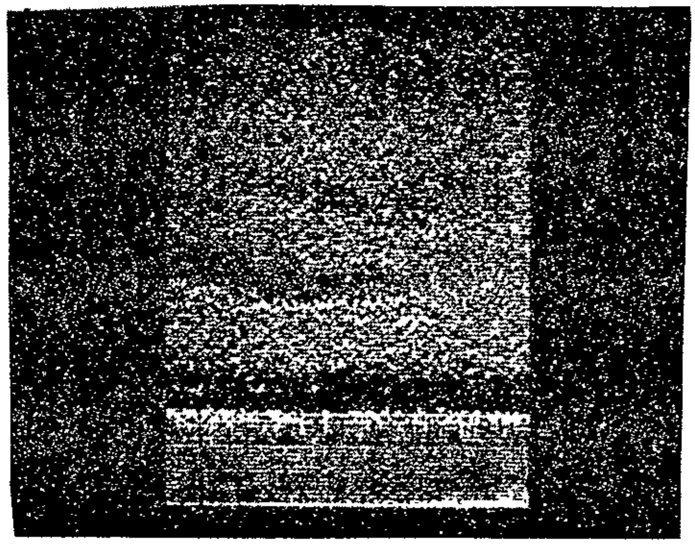

Figure 4-23. Software Simulation Processed Image (Data From Ames Flight-Goldfield Run No. 4).

ORIGINAL PAGE IS OF POOR QUALITY

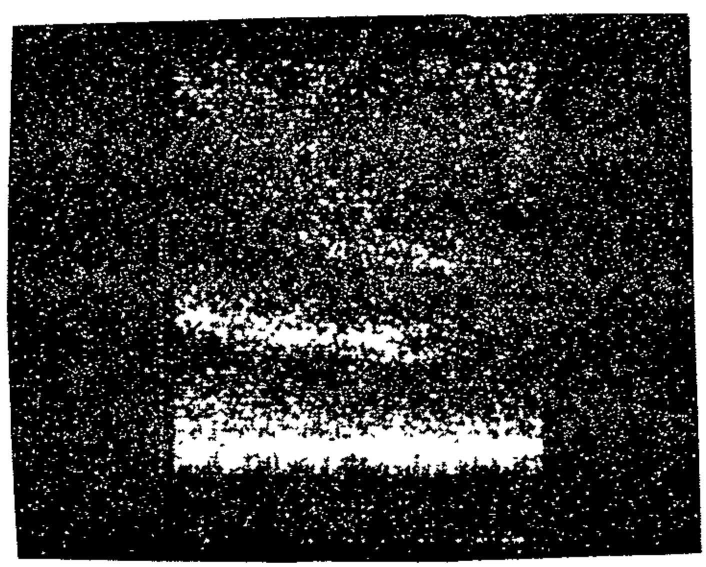

Figure 4-24. Software Simulation Processed Image With Modified Range/Azimuth Filter Tap Weights (Goldfield Run No.4)

Table 4-2

MODIFIED RANGE FILTER TAP WEIGHTS

	COSINE	SINE
1.	399	51
2.	211	40
3.	269	- 2
4.	313	- 90
5.	310	-230
6.	213	-405
7.	- 19	-541
8.	-372	-521
9.	-711	-230
10.	-787	314
11.	-382	833
12.	387	853
13.	907	146
14.	515	-756
15.	-563	-790
16.	-1006	285
17.	- 37	1045
18.	930	203
19.	177	-871
20.	-920	-136
21.	-123	902
22.	761	- 18
23.	-293	-635
24.	-532	490
25.	511	282
26.	-103	-463
27.	-359	355
28.	338	94
29.	-227	-189
30.	- 38	296
31.	220	-300

Table 4-3

MODIFIED AZIMUTH FILTER TAP WEIGHTS

	COSINE	SINE
1.	-781	64
2.	-588	-44
3.	-537	35
4.	-457	105
5.	-353	155
6.	-234	180
7.	-107	179
8.	17	153
9.	133	107
10.	236	46
11.	323	- 22
12.	392	- 91
13.	446	-153
14.	483	-205
15.	507	-242
16.	519	-261
17.	519	-261
18.	507	-242
19.	483	-205
20.	446	-153
21.	392	- 91
22.	323	- 22
23.	236	46
24.	133	107
25.	17	153
26.	-107	179
27.	-234	180
28.	-353	155
29.	-457	105
30.	-537	35
31.	-588	- 44
32.	-781	64

APPENDIX A

DIGITAL PRESUM

FILTER DERIVATION

Filter Specification: -Second order Butterworth Low Pass

-Cutoff Frequency: $f_c = 10.882$ Hz

-Sampling Frequency: $f_s = 1000$ Hz => $T = 10^{-3}$ sec

Second Order Butterworth Transfer Function:

$$H(S_n) = \frac{1}{S_n^2 + \sqrt{2}\, S_n + 1}$$

$$S_n = \frac{S}{\omega_c} \Rightarrow H(s) = \frac{\omega_c^2}{S^2 + \sqrt{2}\,\omega_c S + \omega_c^2}$$

$$H(S) = \frac{\omega_c (j/\sqrt{2})}{S + \omega_c (1/\sqrt{2} + j/\sqrt{2})} + \frac{\omega_c (-j/\sqrt{2})}{S + \omega_c (1/\sqrt{2} - j/\sqrt{2})}$$

where S_n = Normalized Frequency

Second Order Butterworth: Bilinear Transform

$$H(s) = \frac{\omega_c^2}{S^2 + \sqrt{2}\ \omega_c S + \omega_c^2} = \frac{K}{S^2 + aS + b}$$

$$H(z) = H(s)\Big|_{s=\frac{2}{T}\left(\frac{1-Z^{-1}}{1+Z^{-1}}\right)} = \left\{\frac{KT^2}{4 + 2aT + bT^2}\right\} \cdot$$

$$\left\{\frac{(1+Z^{-1})^2}{1 + \left[\frac{2\ (bT^2-4)}{4+2aT+bT^2}\right]Z^{-1} + \left[\frac{4-2aT+bT^2}{4+2aT+bT^2}\right]Z^{-2}}\right\}$$

where: $\omega_c = \frac{2}{T}\tan\frac{\omega_d T}{2} = \frac{2\alpha}{T}$

$$a = \sqrt{2}\ \omega_c = \frac{2\sqrt{2}\ \alpha}{T}$$

$$b = \omega_c^2 = \frac{4\alpha^2}{T^2} = K$$

$$\Rightarrow H(Z) = \left\{\frac{\alpha^2}{1+\sqrt{2}\alpha+\alpha^2}\right\}\left\{\frac{(1+Z^{-1})^2}{1+\left(\frac{2(\alpha^2-1)}{1+\sqrt{2}\alpha+\alpha^2}\right)Z^{-1} + \left(\frac{1-\sqrt{2}\ \alpha+\alpha^2}{1+\sqrt{2}\ \alpha+\alpha^2}\right)Z^{-2}}\right\}$$

For: $F_d = 10.882$ Hz , $\alpha = \tan\left(\frac{2\pi\ F_d T}{2}\right) = .0342$

$T = 10^{-3}$

$$H(Z) = (.0011144)\left(\frac{1+2Z^{-1}+Z^{-2}}{1-1.90338\ Z^{-1} + .907833\ Z^{-2}}\right)$$

ORIGINAL PAGE IS
OF POOR QUALITY

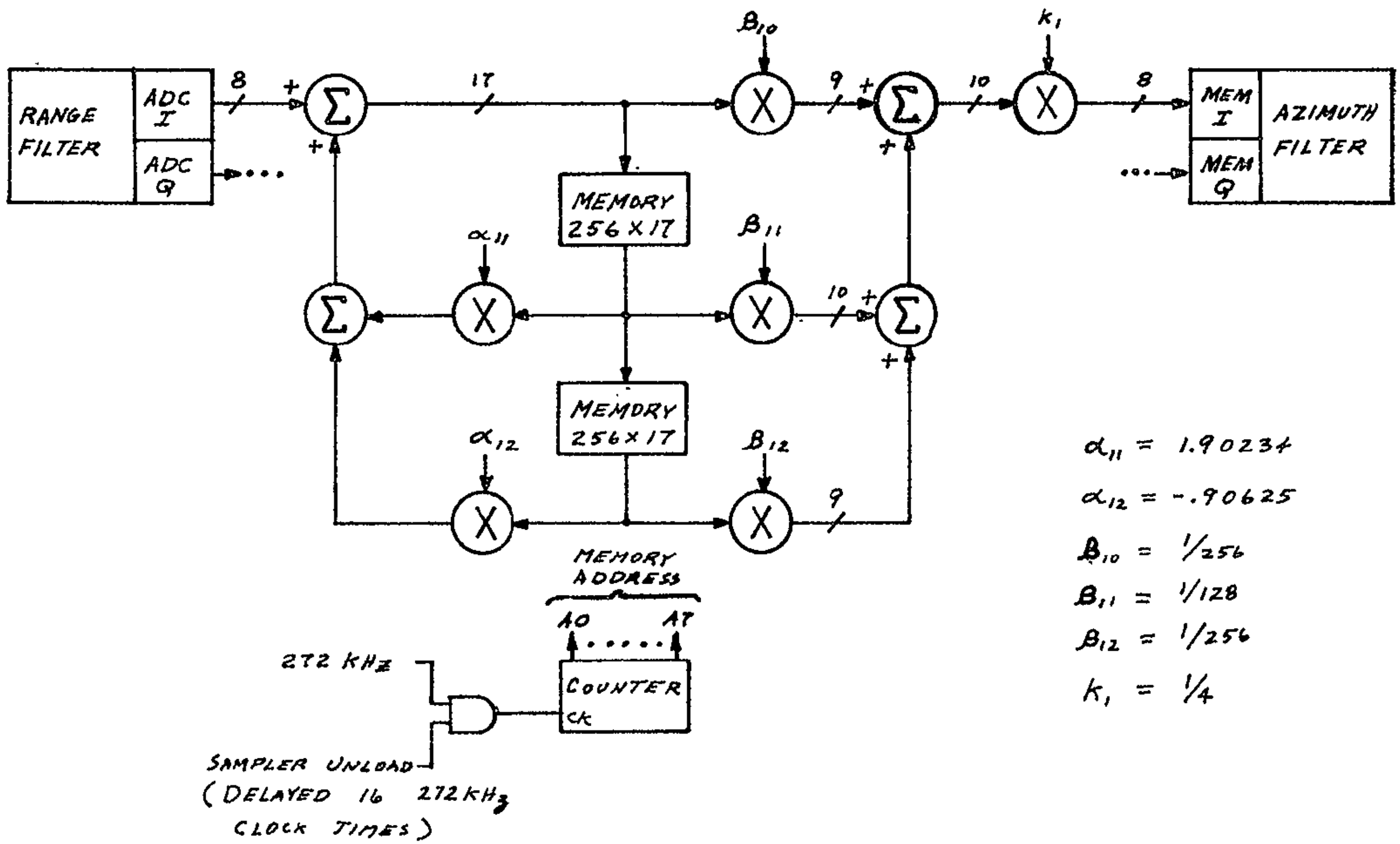

Figure A-1. Digital Presum Filter
(2 Pole Butterworth-Bilinear Transform)

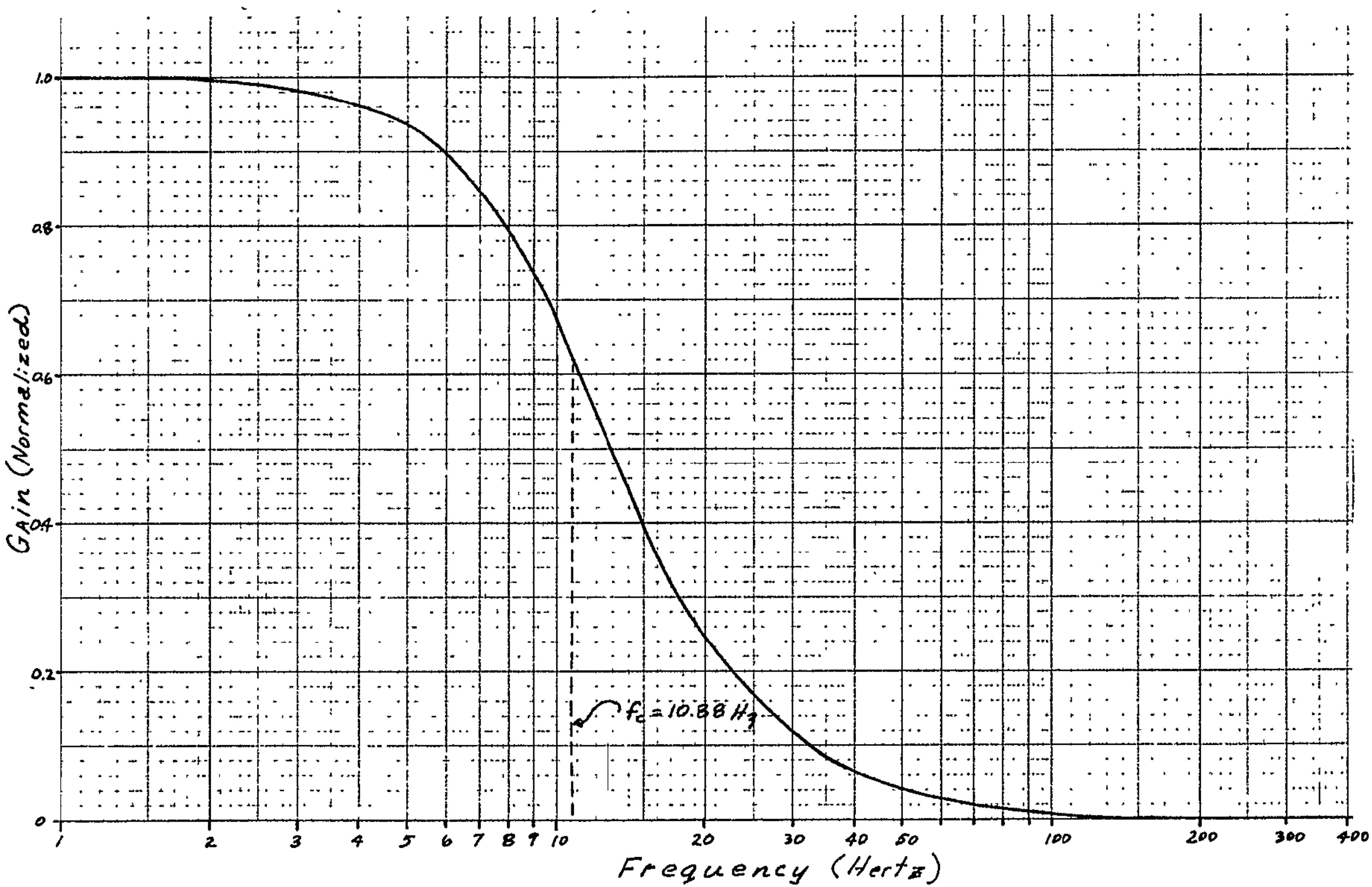

Figure A-2. Magnitude vs. Frequency
- Digital Presum Filter

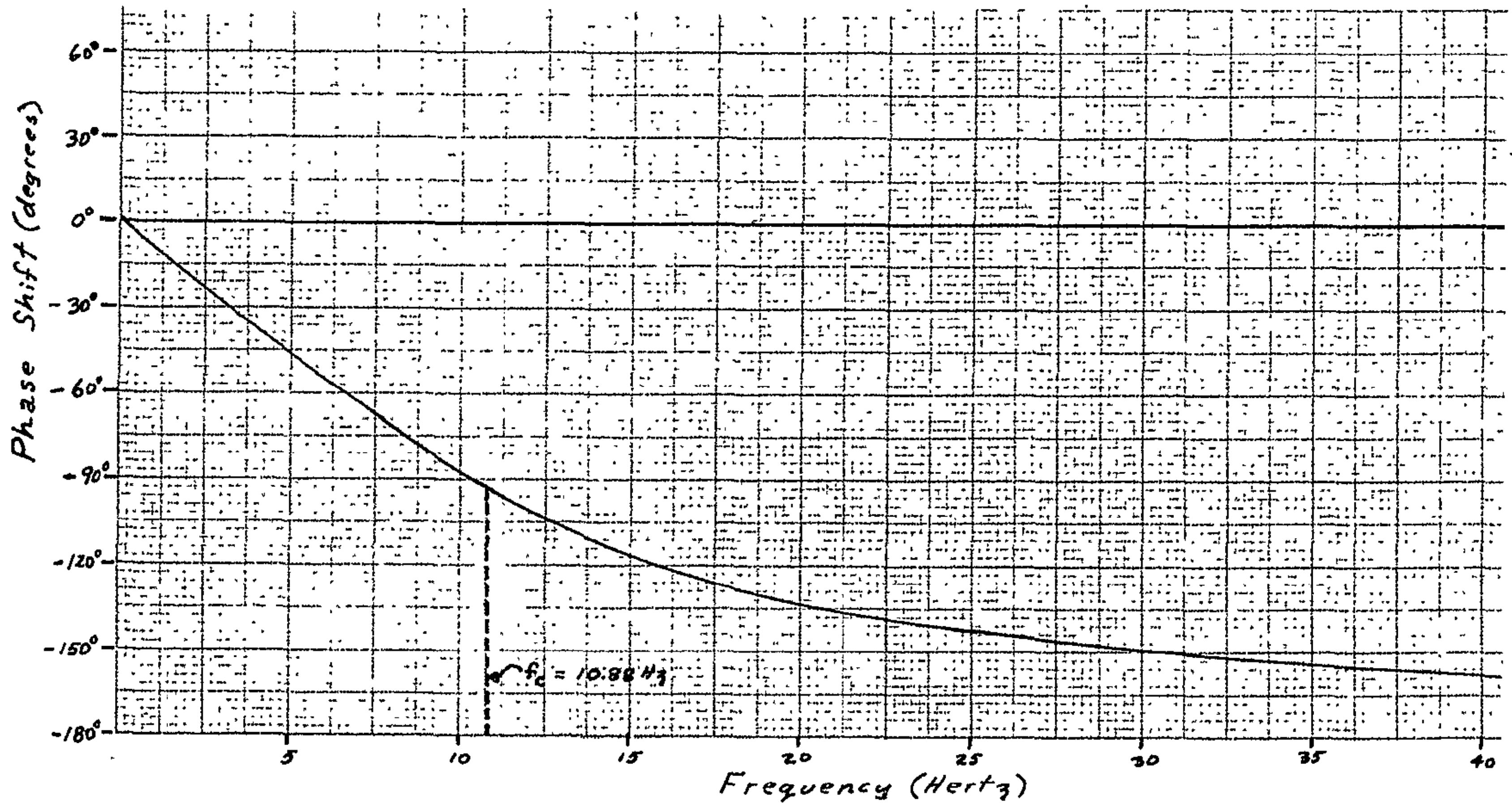

Figure A-3. Phase Shift vs. Frequency - Digital Presum Filter

APPENDIX B

A SYNTHETIC APERTURE
PROCESSOR USING CCD
SIGNAL PROCESSING TECHNIQUES

The following paper was presented at the Conference on CCD Technology and Applications, November 30 - December 2, 1976, Washington DC.

A SYNTHETIC APERTURE PROCESSOR USING CCD SIGNAL PROCESSING TECHNIQUES

By

W.H. Bailey, M.S. Bergath, J.F. DuBose
W.L. Eversole, J.H. McGehee, R.V. Ridings,
and D.C. Young

Texas Instruments Incorporated

ABSTRACT. The synthetic aperture concept has been known since the early 1950's. Application of the concept has been quite limited due to practical implementation difficulties. Early techniques relied upon photographic film for storage. This exposed film was subsequently developed and used in conjunction with an optical correlator which produced the imagery. The development of integrated circuit technology has made it possible to perform the convolution and storage functions in alternate ways. Only in this decade has it been possible to perform real time SAR processing on board an aircraft. Further reductions are still required in order to meet size, weight, and power objectives for most aircraft and satellite applications. The application of charge coupled devices offers significant advantages in these areas in addition to providing a capability to perform operations in an analog domain.

I. INTRODUCTION

Synthetic aperture radar (SAR) imaging appears to be the most suitable technique for achieving high resolution imagery through atmospheric cloud cover. This feature is important for planetary as well as earth orbiting satellite systems, and for military aircraft applications. Such applications require onboard data processing or wide-band data transmission systems in order to handle the large amounts of raw data produced by such systems. Onboard optical correlators of the conventional nature are unattractive for such applications due to size, mechanical stability problems, and long term operational objectives. Digital techniques offer some hope for onboard processing. However, size and power limitations for this approach currently exist. The charge coupled device promises important reductions in size, power, and weight in the implementation of onboard processors.

One of the first scheduled uses of a satellite borne SAR will be SEASAT-A which is to be launched in 1978. The mission of the SAR will be all-weather imaging of the sea for weather forecasting purposes.

A number of techniques have been utilized in implementing SAR processors. Frequency filtering and Fourier transform operations using both optical and digital techniques have been utilized in SAR processing.[1,2] Most approaches store the data in range lines and read the accumulated data from a given range bin into either a filter or transforming equipment which selectively passes the energy within a selected doppler frequency range. The zero doppler frequency generally corresponds to the point broadside a moving aircraft for clutter locked systems, and is the most commonly utilized frequency component analyzed. Optimal detection criterion would require pulse compression of the doppler chirp waveform found along the azimuthal direction.[3]

Generally speaking, when an image of some physical characteristic is needed, the resolution in the two orthogonal directions should be approximately equivalent. This presents a problem to conventional radar sets which could be used to produce an image of the radar cross section of a section of terrain. The resolution of the conventional radar in the radial direction depends directly on signal bandwidth. Pulse-compression techniques permit signal bandwidth to be expanded with negligible sensitivity loss so that adequate range resolution may be realized for many imaging applications.

Azimuth resolution is a more difficult matter, however. Conventional radar azimuth resolution depends ultimately upon the antenna beamwidth.[1] The antenna beamwidth is reduced by increasing the size of the aperture, increasing the carrier frequency, or both. For long-range imaging, however, this approach cannot provide an azimuth resolution that can be realized easily with modern pulse-compression techniques.

The solution to this dilemma is provided by SAR's in which data processing capability is traded for aperture size. In principle, there is no difference between:

An extremely large real antenna, and

A small real antenna that successively occupies all the positions that would be occupied simultaneously by the large real antenna, provided

The data that are successively collected by the small antenna are properly stored and subsequently combined in a simulation of the large real antenna.

Assuming this condition is satisfied, it is possible for a small antenna to move past a scene and record echo data to permit comparable range and azimuth resolution to be realized in an image of the scene after the recorded data have been properly processed, as indicated in Figure 1.

II. DESIGN CONSIDERATIONS

The use of charge coupled device transversal filters provides a very powerful computational tool in the implementation of the correlators required in a SAR processor.

The CCD filters utilized in these experiments are four-phase surface channel devices having split electrode weighting.[4] Initial device concerns were CTE effects, leakage current, and high frequency operation. Early measurements and analysis[5] indicated these effects are minimal for this application. The laboratory feasibility breadboard utilized existing chirp filter designs having time bandwidth (TW) products of 62 and 16 for the range and azimuth correlators, respectively. Table 1 indicates the system parameters of the breadboard. Representative system parameters derived from these filter characteristics are indicated in Table 1 using the procedure outlined in Reference 5. The filters for the engineering model were designed using this procedure to be compatable with the system parameters for an existing JPL radar used for flight experiments. The key parameters for this system are indicated in Table 2.

Table 1. Breadboard Radar/Platform Parameters

Altitude	5.0 km
Slant Range	10.0 km
Nadir angle	60.0 degrees
Velocity	320.0 m/s
Wavelength	32.0 cm
Frequency	936.84 MHz
Transmitted pulse duration	3.58 μs
Transmitted signal bandwidth	17.32 MHz
Slant-range resolution	8.66 m
Along-track ground resolution	10.0 m
Cross-track ground resolution	10.0 m
Range time bandwidth product	62
Range correlation time	0.47 ms
Azimuth time bandwidth product	16
Azimuth correlation time	0.5 s

Table 2. Engineering Model Radar/Platform Parameters

Altitude	10.058 km
Slant range	15.5 m
Nadir angle	39 degrees
Velocity	257 m/s
Wavelength	24.7 cm
Frequency	1215 MHz
Transmitted pulse duration	1.25 μs
Transmitted signal bandwidth	10 MHz
Slant range resolution	15.5 m
Along-track ground resolution	25.1 m
Cross-track ground resolution	24.7 m
Range time bandwidth product	12.5
Range correlation time	58.9 μs
Azimuth time-bandwidth product	2.7
Azimuth correlation time	25.6 μs

Some limitations in the use of CCD transversal filters do exist. Peripheral circuitry limitations such as amplifier slew rates and sampling feed-through currently limit useable data rates to less than 5 MHz. Practical filter lengths are presently limited to less than 1000 stages[6], although some flexibility exists in trading bar size for filter lengths. Several techniques, such as time expansion and presumming may be utilized to extend the operation of a processor utilizing CCD transversal filters.

The achievement of high range resolution implies the use of wideband chirp signals for a pulse compression radar. The use of a surface wave device range chirp correlation filter is an alternative capable of accommodating the required bandwidths. However, the time windows commensurate with the achievable range resolution are typically tens of nanoseconds, and are difficult to handle with A/D conversions and digital techniques.

The use of a modular processor concept in which each module processes on the order of 200 range cells, makes it possible to sample the radar video at a high rate during a small time window corresponding to the module's swath width once each PRI. The number of samples to be stored is the number of samples required to cover the swath plus the number of bits in the range correlator. While the input sampling rate is constrained by Nyquist considerations, the output data rate is constrained by the PRI making time expansion of the video possible in order to reduce the processor module's data rate to one commensurate with CCD transversal filter operation. Subsequent processing speeds may easily be handled with present CCD technology. Another advantage of such a buffering technique is that radar data from an appropriate range swath may be recorded on a conventional instrumentation tape recorder having a few hundred kilohertz bandwidth.

Presumming is an attractive alternative to minimizing the filter lengths and data rates required in the azimuth correlators. Presumming is the process whereby several consecutive samples from a given range bin are combined into one sample for subsequent processing. Presumming ahead of the azimuth correlator is possible in most cases, since the PRF greatly exceeds the azimuth time bandwidth product resulting in considerable oversampling.

Aliasing in the presum operation is a significant potential problem. Aliasing of the doppler components about harmonics of the PRF is inherent since the radar system is a sampled-data system. The antenna characteristics form a filter for the doppler returns due to the geometrical relationship between the antenna pattern and the locations of sources of higher doppler frequencies. However, the relatively large antenna beamwidth again causes ineffective filtering of the higher frequency components. Since presumming amounts to resampling the data at a lower data rate, these higher aliased frequencies must be removed by filtering in order that the new sampling operation not fold them into the video band of interest. This may be accomplished by incorporating a low pass filter into the presum operation.

Focusing is an important consideration in SAR's which involves degradation of resolution as a function of range. It is convenient in Figure 2 to think of a stationary radar with target motion being a straight line as shown. Using conventional terminology, time t is zero when the target is at the point of closest approach. This minimum range value is called R_0.

Data are assumed to be available from the time that the target enters the 3-dB beamwidth point of the real aperture until it leaves the 3-dB beamwidth point on the other side.

At time t, the target is seen in Figure 2 to be displaced a distance Vt from the point of closest approach. The range as a function of time is given by

$$R(t) = (R_0^2 + V^2t^2)^{\frac{1}{2}} \tag{1}$$

For most cases of interest, the distance Vt in Figure 2 is much less than R_0, so that

$$R(t) \approx R_0 \tag{2}$$

Degradation in resolution occurs when this assumption becomes invalid.

The effects of defocusing can be analyzed in terms of chirp slope mismatch degradation as outlined by Cook and Bernfeld.[7] The time bandwidth product of the azimuth chirp waveform for the unweighted case may be determined from[6]

$$TW_{AZ} = \frac{0.405\ \lambda R_0}{\delta_{AZ}^2} \tag{3}$$

where λ is the radar carrier wavelength, R_0 is the range in meters, and δ_{AZ} is the azimuth resolution in meters.

If the filters are assumed matched at the center of the swath, the above equations may be used to determine the differences in time bandwidth products between the nominal value at the center of the range swath, and the near and far extremities of the swath. Analysis of the SEASAT geometries indicate a focusing degradation of approximately 2% could be anticipated over the 100 km swath width for 50 m resolution.

III. LABORATORY BREADBOARD

The first of the two breadboard SAR processors constructed at Texas Instruments in conjunction with this effort is a laboratory model which was developed around existing CCD filter designs. This breadboard simulates the operation of a filter bank approach to the azimuth correlators.[8] A block diagram of the laboratory breadboard is shown in Figure 5.

A single azimuth correlator was constructed which is sequentially stepped through the 200 range bins with a minicomputer in order to minimize hardware construction. The radar/platform parameters for this breadboard system shown in Table 1, are relatively representative of an aircraft radar environment. Range and azimuth correlation is accomplished with Hamming weighted linear FM complex filter pairs having TW products of 62 and 16, respectively. Range and azimuth correlation times are 0.47 ms and 0.5 s, respectively.

In order to form a 200-by-200-element picture with this breadboard, a TI 960A computer with 28K memory used in conjunction with a 1,100,000 word disk memory and a nine-track, 800-BPI magnetic tape unit were used. The simulated radar echo pulses were transferred from the tape to the disk. The simulated radar bursts correspond to radar returns from a swath of interest at sequential azimuthal locations. By recirculating this sequence of bursts to the breadboard while sliding the azimuth read-in time window across the swath time, a complete picture can be processed an azimuth column at a time. To reconstruct the picture, the output of the azimuth correlator is digitized and stored in memory. The memory can then be used much as a scan converter to refresh a CRT display.

The time required to process a 200 x 200 element picture is 1 1/3 hours due to the long azimuth correlation time. Real time processing could be accomplished by expanding the system to 200 azimuth correlators.

A number of test images have been processed with this breadboard. Two of the more significant images are shown in Figures 3 and 4. The upper photographs of Figure 3 indicate a portion of the uncompressed video signal corresponding to 48 point targets arranged in four rows in the range dimension. The point targets have a random signal phase and increase in intensity along the azimuth direction in 2-, 4-, 6-, and 8-percent increments for each of the range rows. Since the range and azimuth TW products are different, each point target's uncompressed video appears as a set of concentric ellipses. Compressing this video with the breadboard reconstructs the point targets as shown in the lower portion of Figure 3.

A second image was processed from an ERTS photograph, which was optically scanned with a microdensitometer, with the resulting picture element intensities stored on a computer tape. A decompression operation was then carried out on the minicomputer which convolved each picture element with a two dimensional chirp similar to that corresponding to a point target in Figure 3, and superimposed the resultant waveforms from picture elements having overlapping correlation functions. These decompressed data were then compressed utilizing the CCD breadboard and a compression program written for the minicomputer. Figure 4 reveals a 400 x 400 image which was processed as four 200 x 200 images.

A few subtle problem areas have been discovered in the process of evaluating this breadboard. The processed picture of Figure 4 indicates an intensity shading from left to right which is due to insufficient low frequency response in the ac coupling network at the squaring converter input. Efforts to direct couple this node were unsuccessful due to the thermal drift problems associated with the prior circuitry and the sensitivity of the analog multiplier to a precise null. An additional problem concerning dynamic range was encountered in processing the simulated pictures. A normalized 8 bit encoding scheme was used in the minicomputer data handling hardware. Since the point target test pattern of Figure 3 has non-overlapping correlation functions, the input waveforms are similarly non-overlapping, resulting in minimal amplitude reduction in the normalization process. However, the composite decompressed waveforms from the ERTS photograph of Figure 4 are formed by the superposition of two dimensional chirp waveforms from a large number of adjacent point targets. Normalization of this composite waveform to 8 bits makes the quantization error significant relative to the maximum chirp amplitude from a single picture element. As a result, the signal-to-noise ratio of many of the picture elements is relatively low. The dynamic range goal in the design of this breadboard was approximately 40 dB and was crudely based upon conventional TV grey scale detectability. The dynamic range of the breadboard was limited by the analog multipliers which perform the squaring function to approximately 40 dB. Additional dynamic range for the processor and test system would be desirable, but the desired increase is difficult to quantitatively assess.

IV. AIRCRAFT ENGINEERING MODEL

The aircraft engineering model, indicated in Figure 6 which is currently being constructed, is designed to match the system parameters of a radar utilized for SAR experiments on a CV-990 aircraft. This breadboard will be capable of real time SAR processing onboard the aircraft. The architecture of this breadboard differs from that of the earlier version by utilizing a digital "corner-turning" memory as opposed to the filter bank approach previously simulated. The primary justification for this choice was a short term economic consideration.

This breadboard utilizes a CCD delay line time expander to acquire approximately 500 range samples at a 25 MHz rate from the appropriate range swath each PRI. These samples are unloaded at a relatively slow rate (543 KHz) reducing the speed requirements of the remainder of the processor and making it possible to record unprocessed data from the desired swath on a conventional instrumentation tape recorder. This input sampler and recorder have been flown and data recorded for laboratory test purposes. This data will be played back into the range correlator which requires only a I and Q filter, since this radar system utilizes a frequency offset linear FM waveform. The output of this correlator is then digitized. The signals subsequently enter presum filters having 2nd order Butterworth low pass responses and presum numbers of 8. The data are then stored in the "corner-turning" memory in range lines (constant azimuth) and are read out in range bins (constant range). The "corner turning" memory's outputs drive digital to analog converters which supply inputs to the azimuth correlator producing a compressed image line along the azimuth direction. This output is again digitized and subsequently applied to a digital scan converter which stores the data and uses it to refresh the CRT display.

The CCD correlators for the aircraft engineering model utilize a weighting coefficient modification of an existing bar design to produce a 32 stage frequency offset chirp and chirp-through-zero filter pairs for the range and azimuth correlators, respectively. The filter characteristics utilized in the design of these devices were derived from the parameters of the CV-990 radar to be utilized in the flight experiments. Table 2 lists many of the important system parameters. Figure 7 indicates the impulse and correlation characteristics of these filters. System operating frequencies for these correlators were 543 KHz and 1.25 MHz for the range and azimuth correlators, respectively.

V. CONCLUSIONS

The use of CCD's in onboard SAR processors appears to offer tremendous advantages through the powerful computational equivalency of transversal filters and the high density achievable with either analog or digital memories.

The two architectural approaches considered in this paper have numerous advantages and disadvantages. The filter bank processor utilizes CCD filters for both signal storage and convolution calculation eliminating the need for a large memory. CCD data rates with this configuration are minimal, since data is transferred at the PRF (or lower if presumming is utilized). Many filters are required to implement a system covering a large number of range bins. However, the feasibility of integrating multiple complex correlators on a single chip has been demonstrated.[8] Storage times and gain uniformity are additional concerns for the filter bank approach.

The "corner-turning" memory approach requires only a single azimuth correlator through which data is multiplexed. Storage time in the correlator becomes inconsequential, but operating speeds may become quite high for some systems. Redundant memories are likely to be required due to load/unload difficulties. Storage times within the memory may be a concern with this architecture. Although this configuration appears quite simple in block diagram form, control and addressing logic may become significant relative to the remainder of the system.

Improvements in SAR processors may be expected in the areas of improved resolution, multiple look imagery, focusing, motion compensation, and wider dynamic range. Techniques for accomplishing these improvements will likely influence the architecture of future processors.

ACKNOWLEDGEMENT

The authors gratefully acknowledge the support of the Jet Propulsion Laboratory through contract numbers 953954, 954087, and 954340 monitored by Wayne Arens.

REFERENCES

1. Brown, W.M., and Porcello, L.T., "An Introduction to Synthetic Aperture Radar," IEEE Spectrum, pp. 52-62, September, 1969.

2. Kirk, J.C., Jr., "A Discussion of Digital Processing in Synthetic Aperture Radar," IEEE Transactions on Aerospace and Electronic Systems, Vol. AES-11, No. 3, pp. 326-337, May 1975.

3. Harger, R.O., Synthetic Aperture Radar Systems: Theory and Design, New York Academic Press, 1970.

4. Buss, D.D., Collins, D.R., Bailey, W.H., and Reeves, C.R., "Transversal Filtering Using Charge Transfer Devices," IEEE J. Solid State Circuits, SC-8, pp. 134-146, April, 1973.

5. Bailey, W.H., Eversole, W., Holmes, J., Arens, W., Hoover, W., McGehee, J., and Ridings, R., "CCD Applications to Synthetic Aperture Radar," Proc. of CCD Applications Conference, San Diego, pp. 301-308, October 1975.

6. Hewes, C.R., "A Self Contained 800 Stage CCD Transversal Filter," Proc. of CCD Applications Conference, San Diego, pp. 309-318, October, 1975.

7. Cook, C.E., and Bernfeld, M., Radar Signals: An Introduction to Theory and Application, New York: Academic Press, pp. 152, 1967.

8. Bailey, W.H., Buss, D.D., Hite, L.R., and Whatley, M.W., "Radar Video Processing Using the CCD Chirp Z Transform," Proc. of CCD Applications Conference, San Diego, pp. 283-290, October 1975.

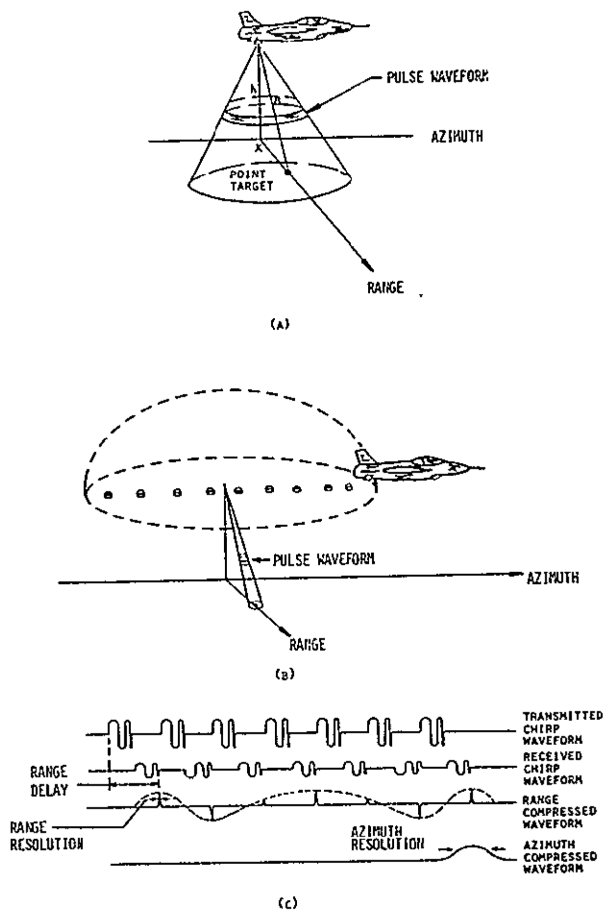

FIGURE 1. SYNTHETIC APERTURE RADAR PROCESSING CONCEPT, SHOWING:
(A) REAL ANTENNA PATTERN, (B) SYNTHETIC ANTENNA PATTERN, AND (C) WAVEFORM PROCESSING.

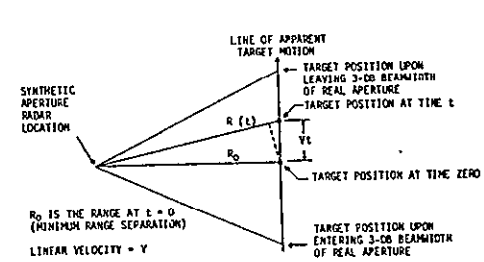

FIGURE 2. BASIC SAR AZIMUTH GEOMETRY

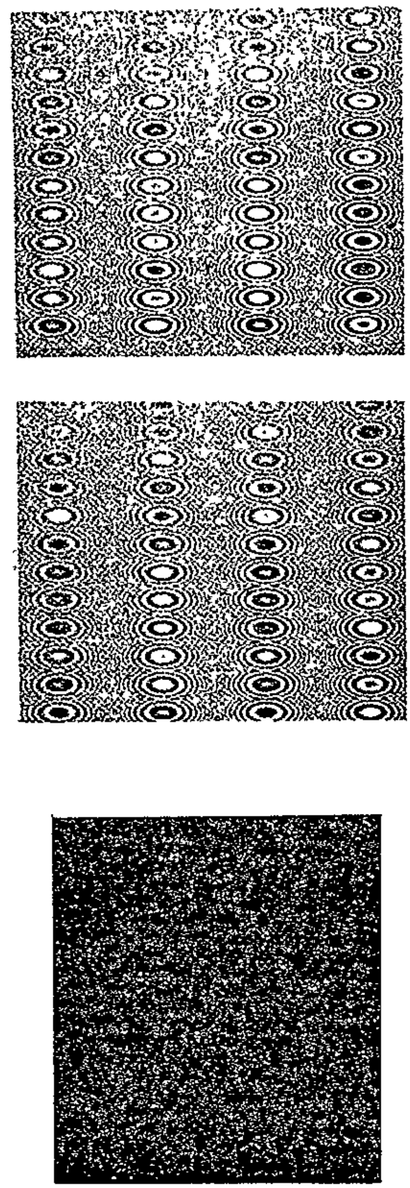

I INPUT

Q INPUT

CCD PROCESSED OUTPUT

FIGURE 3. POINT TARGET AMPLITUDE TEST (48 POINT TARGETS WITH LINEARLY INCREASING INTENSITY, AND RANDOM PHASE)

ORIGINAL PAGE IS OF POOR QUALITY

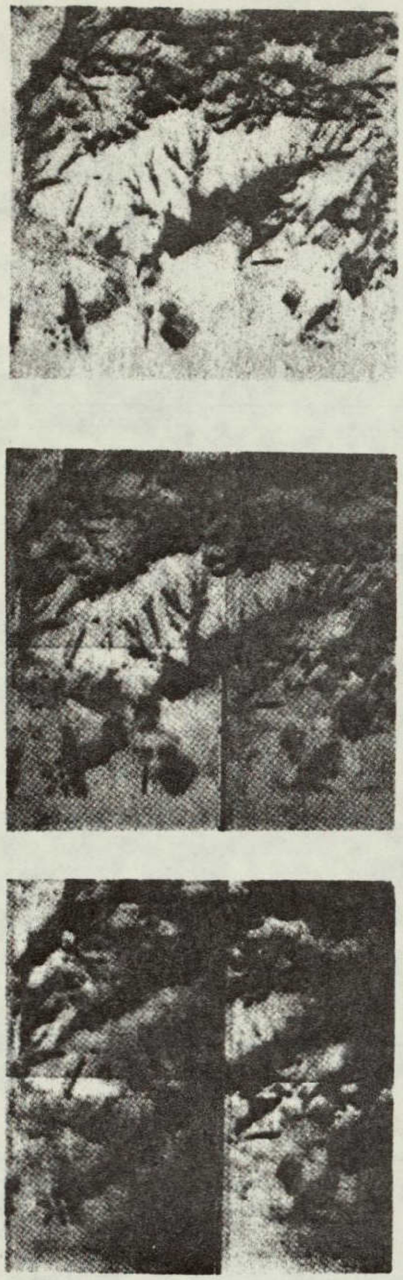

SCANNED IMAGE

DIGITALLY PROCESSED IMAGE

CCD PROCESSED IMAGE

FIGURE 4. IMAGING RADAR MOUNTAIN SCENE (400 x 400)

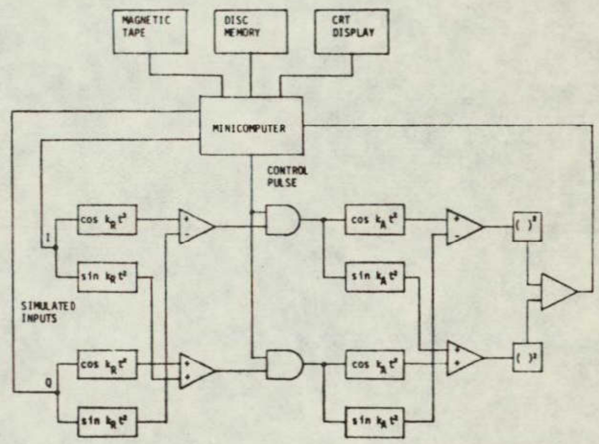

FIGURE 5. LABORATORY BREADBOARD BLOCK DIAGRAM

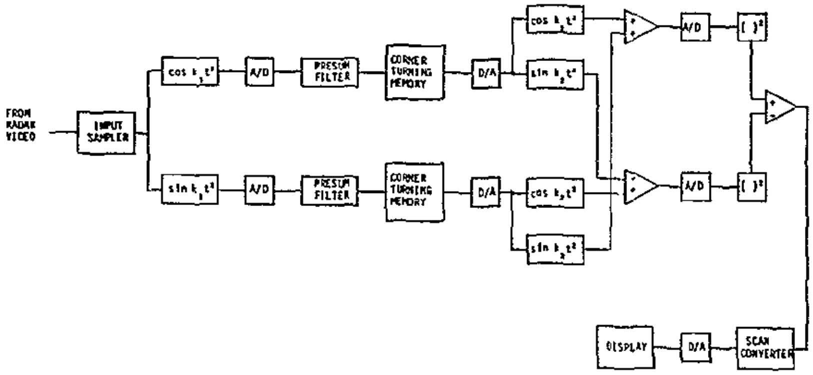

FIGURE 6. ENGINEERING MODEL BLOCK DIAGRAM

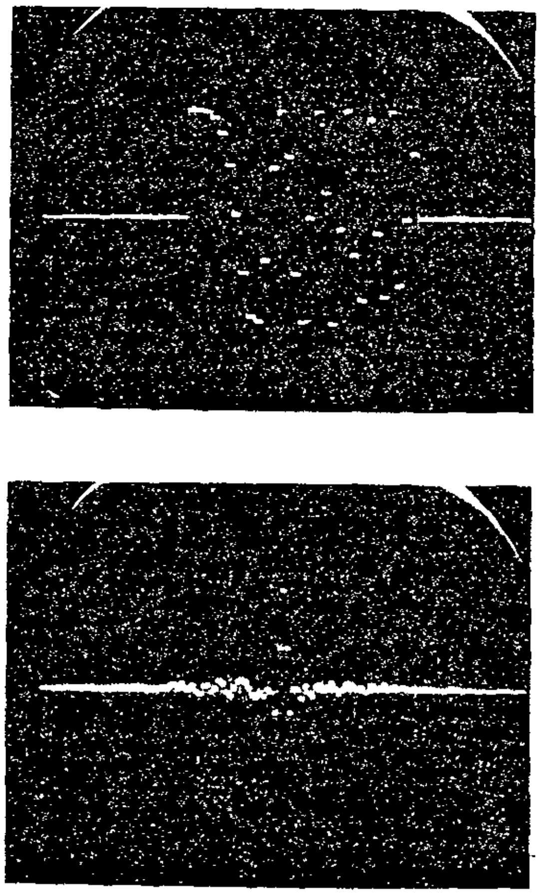

(A)

(B)

FIGURE 7. RANGE FILTER CHARACTERISTICS SHOWING:
(A) INPUT AND (B) OUTPUT

APPENDIX C

EQUIPMENT
PHOTOGRAPHS

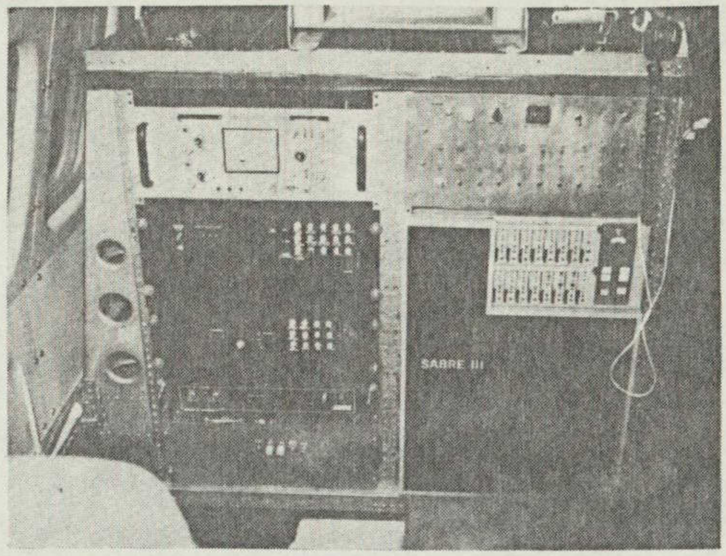

FULL SIZE RACK
CONTAINING SAMPLER/RECORDER

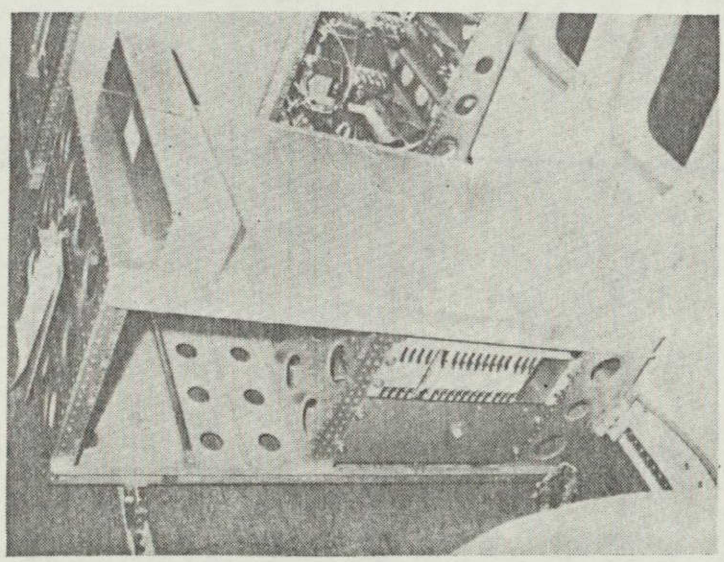

HALF SIZE RACK
CONTAINING TAPE RECORDER/
DESKEW ELECTRONICS

Figure C-1. Input Sampler/Tape Recorder Installation on CV990 Aircraft.

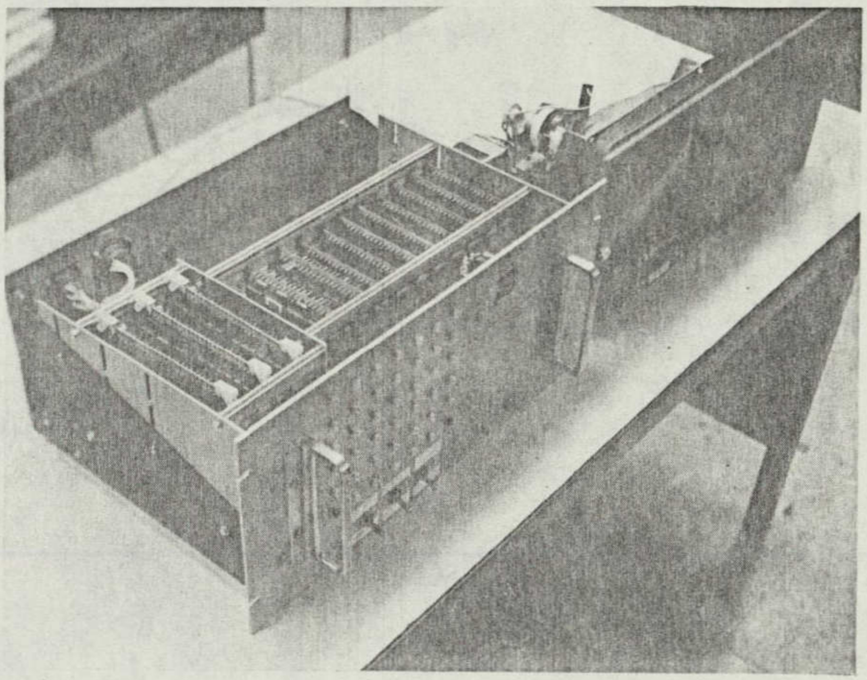

Figure C-2. Scan Converter and Realtime Display

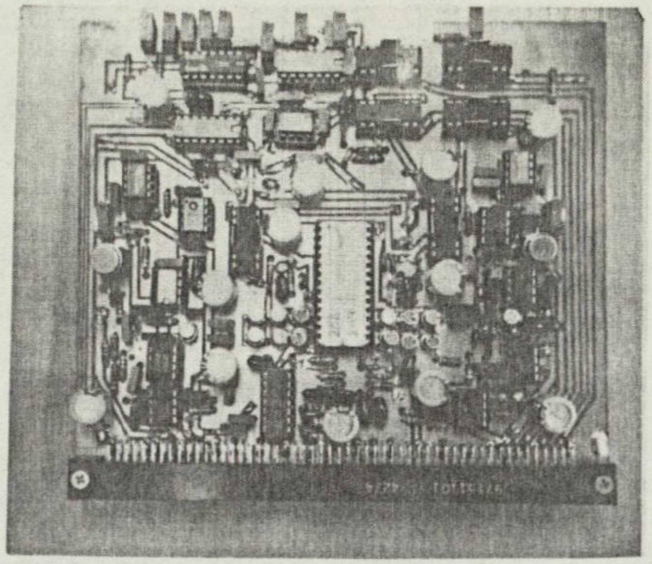

CCD Range Filter

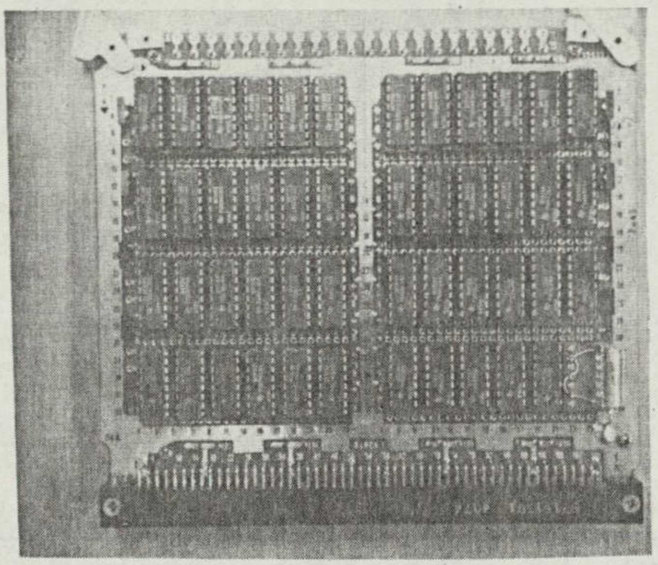

Presum Filter Logic
Board No. 1

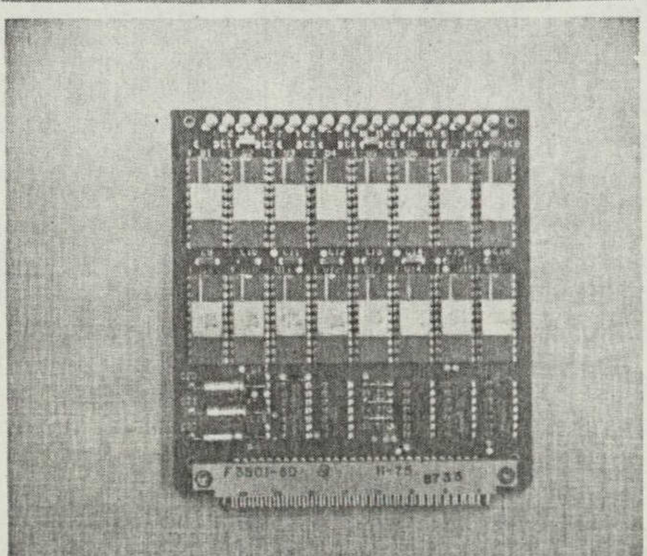

64K Memory

Figure C-3. IPM Circuit Boards

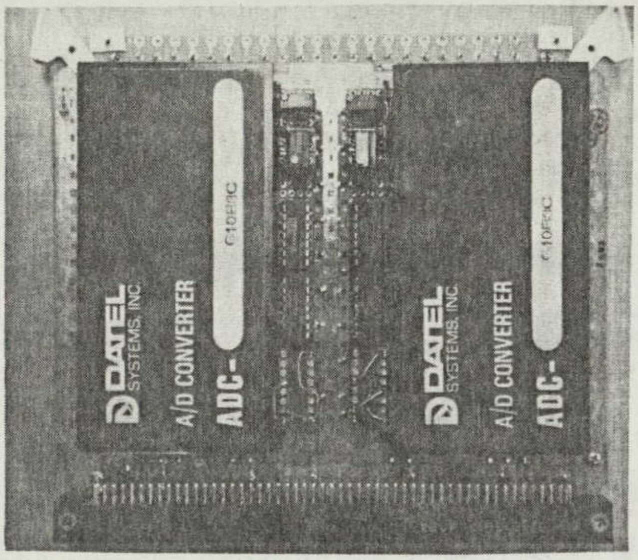

A/D Converters

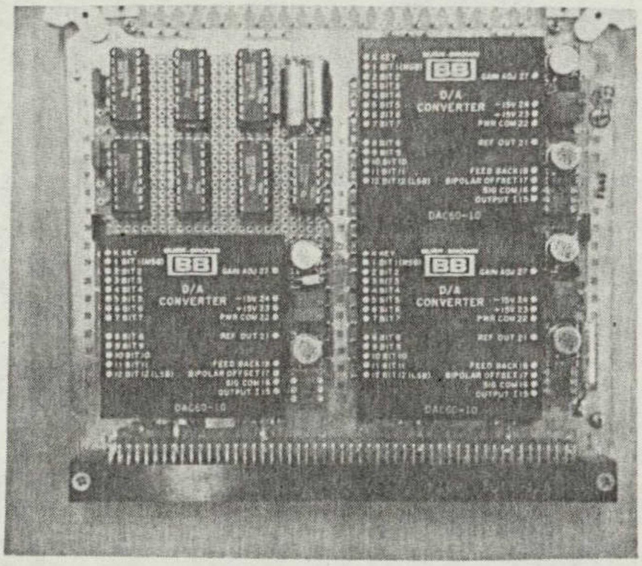

D/A Converters

Figure C-3. IPM Circuit Boards (Con't)